SPECTRAL ANALYSIS AND INTERPRETATION OF AEROMAGNETIC ANOMALIES OVER SOKOTO BASIN, NIGERIA.

By

SAMBO SHEHU OGANIJA

B.Sc   (Hons)   Physics,   Ibadan.

A thesis submitted to the Postgraduate School,
Ahmadu Bello University, Zaria in partial fulfilment
of the requirements for the award of the degree of
Master of Science in Applied Geophysics.

Department of Physics
Faculty of Science
Ahmadu Bello University,
Zaria.

January, 1994

DEDICATION

This work is dedicated to my wife Mrs. Sabityu Sambo Oganija and our children Fadhlat Sambo Oganija, Shakirat Sambo Oganija and Ramata-lahi Sambo Oganija.
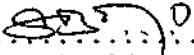
DECLARATION

The report presented in this thesis is not a published, or an unpublished work of another author. It is the result of an original study carried out by this author. To the best of my knowledge, it has not been submitted in whatever form to any other institution, organisation or body other than the Ahmadu Bello University, Zaria for the award of an M.Sc degree in Applied Geophysics. All literature reviewed during the course of this work are duly acknowledged and referenced.

8/2/94
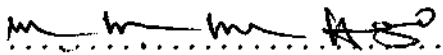
....
S.O. SAMBO

CERTIFICATION

This thesis entitled "Spectral Analysis and Interpretation of Aeromagnetic anomalies over Sokoto Basin, Nigeria" by Sambo Shehu Oganija, meets the regulations governing the award of the degree of Master of Science of Ahmadu Bello University, and is approved for its contribution to knowledge and literary presentation.

....09/02/94....
Prof. S.B. Ojo   Date
Chairman, Supervisory Committee

....09.02.94....
Dr. M.N. Umego   Date
Member, Supervisory Committee
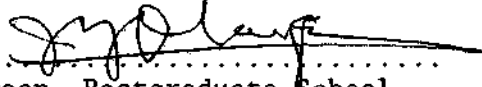
....09/02/94....
Prof. S. B. Ojo   Date
Head of Department

....a/11/95....
Dean, Postgraduate School   Date

ACKNOWLEDGEMENT

during the course of this programme, when my activities appeared to be far removed from the traditional duties of a Senior member of the family. Much thanks and appreciation go to Mallam Ahamed Abdul-wahab, Dr. Dauda Oba and Mr. Bello Shuaib for their friendly assistance.

Lastly, but obviously not the least sincere thanks are due to the Almighty Allah who inspired me into Geosciences and through whose Grace I was able to accomplish this task. "Al-hamudu Lilah."

ABSTRACT

Aeromagnetic data of the Sokoto Basin have been analysed by two-dimensional spectral analysis to determine the lateral variation in the Sedimentary thickness and structures under the basin. The area investigated cover the portion of the basin between latitude 10°30'N and 14°N, longitude 3°30'E and 6°30'E. Spectral depth determinations to magnetic sources in the region gave three depth ranges namely 0.11 km to 0.28 km, 0.50 km to 1.40 km and 0.79 km to 1.85 km. The depths varying between 0.11 km and 0.28 km refer to the contribution by the near surface disturbances, while the deeper depth ranges varying between 0.50 km and 1.40 km refer to a magnetic level corresponding to the basement surface. The depth ranging between 0.79 km an 1.85 km may correspond to the top of structures within the basement. A magnetic depth to basement map revealed that the basement surface is generally shallow and attain a maximum depth of 1.40 km at the centre of the basin. In general, the magnetic data revealed an irregular basement floor resulting from gentle folding of the basement rocks along a general N-S axis. Sediment-filled troughs and depressions on the basement surface have been revealed and these form targets for ground water exploration. The absence of major faulting even at the sediment-basement boundary tend to suggest that the Southeastern sector of the Iullemmeden Basin probably originated from the tectonic movement within the Precambrian basement rocks.

TABLE OF CONTENTS

CHAPTER ONE INTRODUCTION

CHAPTER TWO GEOLOGY OF THE SOKOTO BASIN

LIST OF TABLES

LIST OF FIGURES

LIST OF APPENDICES

CHAPTER ONE

INTRODUCTION

1.1 GENERAL INTRODUCTION

Although many geophysical methods can be used to estimate
depth to bed-rock, each has inherent theoretical or practical
limitations. Results from seismic refraction are inaccurate if
undetected thin or low-velocity layers overlie bed-rock. In some
places compact glacial till has velocity similar to bed-rock.
Measurement using hammers and weight-droppers are difficult or
impossible over thick forest, litter, mud, swamps and
waterbodies. Traffic and wind often create serious interference.
A crew of two is usually needed.

Another common method, resistivity sounding has similar
problems. Materials such as gravel or sandy glacial till may
have resistivities indistinguishable from bed-rock. True
thickness of low resistivity intermediate layer and thus depths
of the underlying layers cannot be determined accurately .
(problem of "equivalence"). Surface conditions such as swamps,
dry sand, ice and frozen ground in temperate regions inhibit or
prevent field work. For maximum efficiency crews of two or four
are needed.

The gravity method is beset with certain disadvantages which
make it unsuitable as reconnaissance method for ore prospecting
in the same sense as electrical methods. The gravity anomalies
produced by even sizeable ore masses are small and often easily
masked by the effects of topographic irregularities, moderate

variations in the thickness and composition of the overburden, regional anomaly trends due to relatively deep seated masses and so on. Gravity surveys are expensive on account of the rather detailed knowledge that is required of topographic heights. The reduction of raw gravity data to usable form, which is needed for bringing out the effect of anomalous masses, also costs time and money.

In contrast, magnetic measurements can be made rapidly by a single person almost anywhere. The overburden, the source of so much difficulty with other methods is frequently insignificantly magnetised; all of the sources are within the bed-rock. With modern techniques, interpretation is very rapid, although as with all geophysical methods it has its limitations. These include problems of noisy data and situations where the basic model does not approximate geology.

1.2 THE SPECTRAL METHOD

Spectral methods of geodata processing and analysis are being increasingly employed, in recent years, in the interpretation of geophysical data partly owing to their elegance in handling large body of data and partly owing to their in-built mechanism for signal-to-noise ratio enhancement. In these methods the characteristics of the observed anomalies are studied by first transforming the data from space to frequency domain and then analysing their frequency characteristics (Bath, 1974). Since magnetic and gravity

anomalies can be conveniently treated as space series amenable to Fourier analysis and synthesis without in any way affecting the intrinsic features of these anomalies, spectral methods provide a powerful approach to their analysis and interpretation. It is, particularly in the case of downward continuation and in the case of source-depth prediction for the layered structures, that the spectral analyses of gravity and magnetic data appear to have been most effective (Spector and Grant, 1970; Hahn, et al., 1976). This is demonstrated in the mapping of magnetic layers in the ultra-mafic body and other geoexploration problems.

1.3 THE SOKOTO BASIN

The Sokoto Basin which is located in the north-western part of Nigeria forms the south-eastern sector of the Iullemmeden Basin. It is situated between latitude $10°30'N$ and $14 N$, Longitude $3°30'E$ and $6°30'E$ (Figure 1.1). This sedimentary basin in north-western Nigeria consist predominantly of a gentle undulating plain with an average elevation varying from 250 - 400 metres above sea level (Kogbe, 1979). This monotonous plain is occasionally interrupted by steep-sided flat-topped hills. A low escarpment, which was named the "Dange Scarp" by earlier workers is the most prominent feature in the basin and is closely related to the geology. The area to the east of this escarpment consists predominantly of a gentle undulating sandy
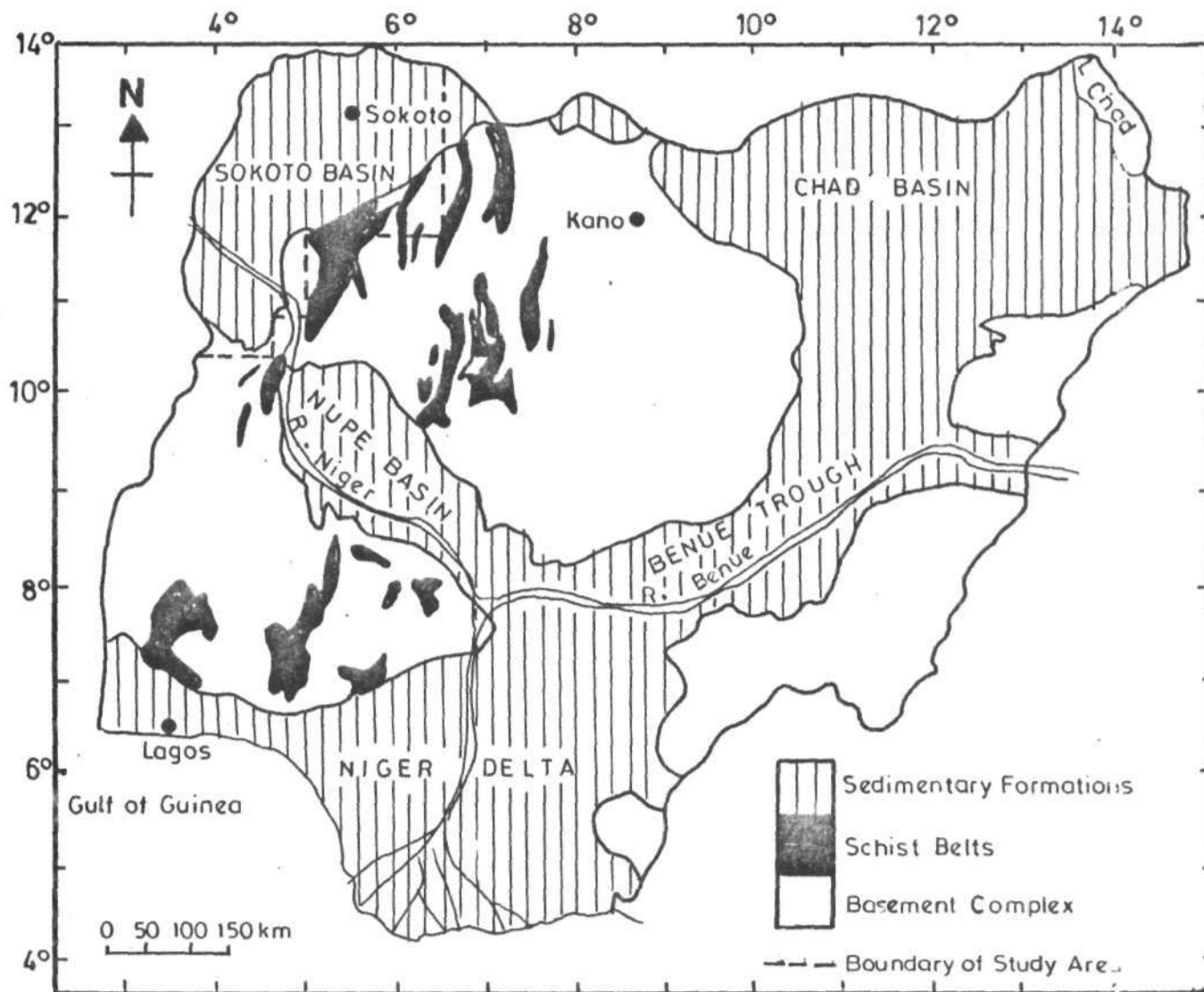
Fig. 1.1: Simplified geological map of Nigeria showing boundary of the study area

plain, which extends south-westwards to the basement complex boundary. The edge of this escarpment is marked with a high drainage density indicating active stream dissection resulting in deeply incised ravines with numerous mesas and outliers scattered on the plain to the east (Kogbe, 1981).

1.4 REVIEW OF PREVIOUS GEOPHYSICAL STUDIES IN THE AREA

In order to understand the present study and to appreciate the need for it, it is instructive to review the geophysical studies that have been carried out in the basin.

The first geophysical investigations in the region was the aeromagnetic mapping which was part of the nation-wide airborne geophysical series carried out for the Geological Survey of Nigeria (GSN). The result of the survey has been published as contour maps on a scale of 1:100,000 which are in the custody of GSN.

Ananaba (1983) carried out a reconnaissance remote sensing study over the entire area of the country north of 8° latitude using LANDSAT images. Two major indicator maps, drainage map and lineament map were compiled and analysed. The lineaments mapped were however not classified as faults, joints, etc., and as such the LANDSAT study would require ground geological and geophysical follow-up. A lineament density map was also compiled and on comparison with the primary mineral map of Nigeria revealed some remarkable correlation between the area of high

lineament density and area of known primary mineral occurrence (Ananaba and Ajakaiye, 1987).

A ground follow-up radiometric survey of some radiometric anomalies delineated from aeroradiometric survey also commissioned by GSN was carried out by Uwa (1984). Attention was paid to three locations with a total area of about 1 km² in the vicinity of Dange village. The locations were considered to have the highest possibility of uranium mineralisation in the Sokoto Basin. The study concluded that the measured uranium concentration were lower than the level normally regarded to be of economic importance.

A few gravity measurements have also been carried out on some major roads in this area. Verheijen and Ajakaiye (1987) established a gravimeter calibration line in this area in which about three stations were located within this survey area. Osazuwa (1985) established a primary gravity network for Nigeria of which five base stations are located within the study area. Due to some deficiencies in Verheijen and Ajakaiye gravimeter calibration line, Osazuwa (1992) established a Nigerian Standard Gravimeter calibration line (NSGCL) from a series of precise gravity measurements made with three Lacoste and Romberg Model gravity meters. The NSGCL extends from Jos in Central Nigeria to Ilella in north western Nigeria thus covering a total distance of about 1,483 km (Osazuwa, 1992).

The geological survey of Nigeria had since the 1930's carried out electrical resistivity, electromagnetic and seismic

refraction surveys in different parts of the basin. The surveys were aimed at studying the aquifers of the basin with a view to selecting favourable sites for ground water boreholes. The results of some of these surveys have been published either as Geological Survey of Nigeria Bulletins or as special publications (Raeburn and Tattam, 1930; Jones, 1984). Unfortunately, only one or two of the numerous boreholes scattered over the basin is known to have reached the basement and as such depth to basement estimates have been by extrapolations.

Recently, Umego (1990) carried out a gravity survey over parts of the basin complemented by the analysis of aeromagnetic data over the basin area. He observed that the area shows an alignment of three linear belts of anomalous magnetic intensities. From the magnetic data, he produced the first depth to basement map of the basin. However, in comparing the results obtained from gravity and magnetic analysis, he noted a significant difference in the depth to basement estimates from both methods, the magnetic depth estimates being generally larger. For example, the maximum depth estimated by the gravity method was 1.0 km at one of the depressions, while the magnetic method yielded a value of 1.4 km at the same location. At another location, comparisons showed estimates of 0.8 km and 1.6 km for the gravity and magnetic methods respectively.

Several factors were suggested as being responsible for these differences. These include errors in the density values

used for the gravity interpretation, the quality of the magnetic data which has been considerably filtered by contouring and re-digitizing process, differences in the countouring and re-digitizing process, differences in the geologic and 'magnetic basement', and the basic assumption of the Werner deconvolution technique used in the magnetic analysis i.e that the magnetic sources are thin dykes or magnetic interface. In concluding his observations, Umego (1990) noted that the differences were significant enough to warrant further investigations. He suggested that boreholes and seismic information would considerably assist in constraining the models.

The present aeromagnetic study is the first attempt at interpreting the aeromagnetic anomalies over the Sokoto Basin by employing techniques based on spectral analysis. Bearing in mind the fact that the aeromagnetic data have been considerably filtered in the process of contouring and re-digitization, a similar filtering technique (spectral analysis) is particularly suitable for the data set because it determines the average depths of an ensemble of magnetic sources and the process of averaging is a smoothing (or low-pass filter) process.

1.5 SCOPE AND OBJECTIVES OF THE PRESENT STUDY

The objectives of the study are as follows:

a) to investigate the lateral variation in sedimentary thickness within the basin using the spectral technique. This has a direct bearing on its hydrocarbon and ground water accumulation potential.

b) to use the results obtained in (a) to prepare the generalised magnetic depth to basement map of the basin and from this make deductions on the structures of the basin.

c) to assess the reliability of the findings by the two-dimensional spectral technique by comparing the results with the depth estimates made by other techniques.

CHAPTER TWO

GEOLOGY OF THE SOKOTO BASIN

2.1 INTRODUCTION

The Sokoto Basin is situated in the North-western part of
Nigeria, between latitude 10°30'N and 14°N, longitude 3°30'E and
6°30'E (Fig. 1.1). The basin is at an elevation ranging from 150
to 850 m above sea level. Most of the area is generally flat
with a gentle hilly area in the south-east.

The basin forms the south-eastern sector of the large,
nearly circular sedimentary basin, generally referred to as the
Iullemmeden Basin of West Africa (Figure 2.1). This basin
(Iullemmeden), extends from Mali and Western boundary of the
Republic of Niger through northern Benin Republic and north-
western Nigeria into eastern Niger (Kogbe, 1981).

2.2 DETAILED GEOLOGY OF SOKOTO BASIN

Figure 2.2 is a simplified version of the geological map of
the basin. In north-western Nigeria, the sediments of the
Iullemmeden Basin were accumulated during three main phases of
deposition, namely, continental Mesozoic and Tertiary phases
(the first and last), with an intervening Maastrichtian to
Paleocene phase (the second). Overlying the Pre-Cambrian
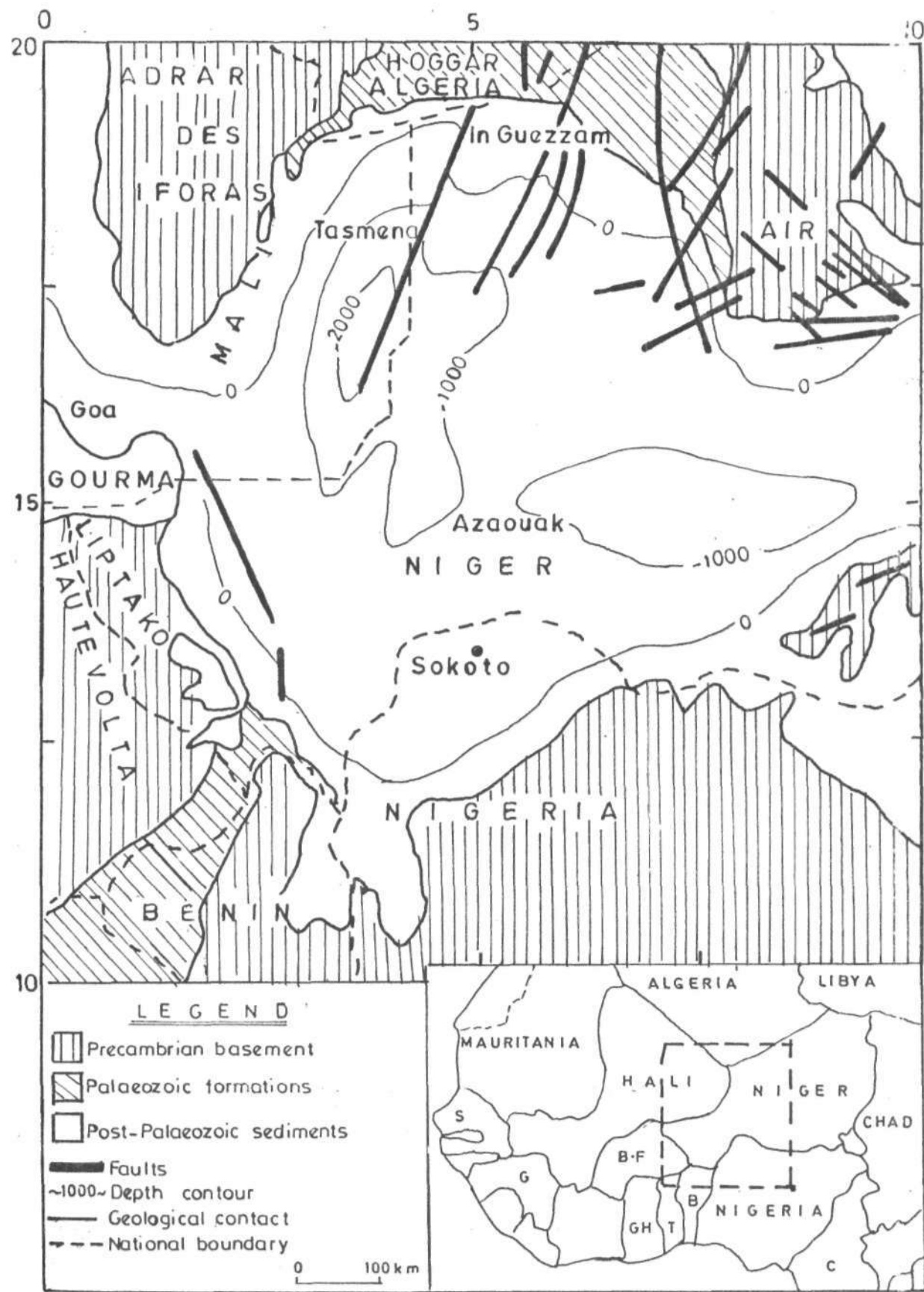
Fig. 2.1: Structural map of the Iullemm eden Basin (After Kogbe, 1981)
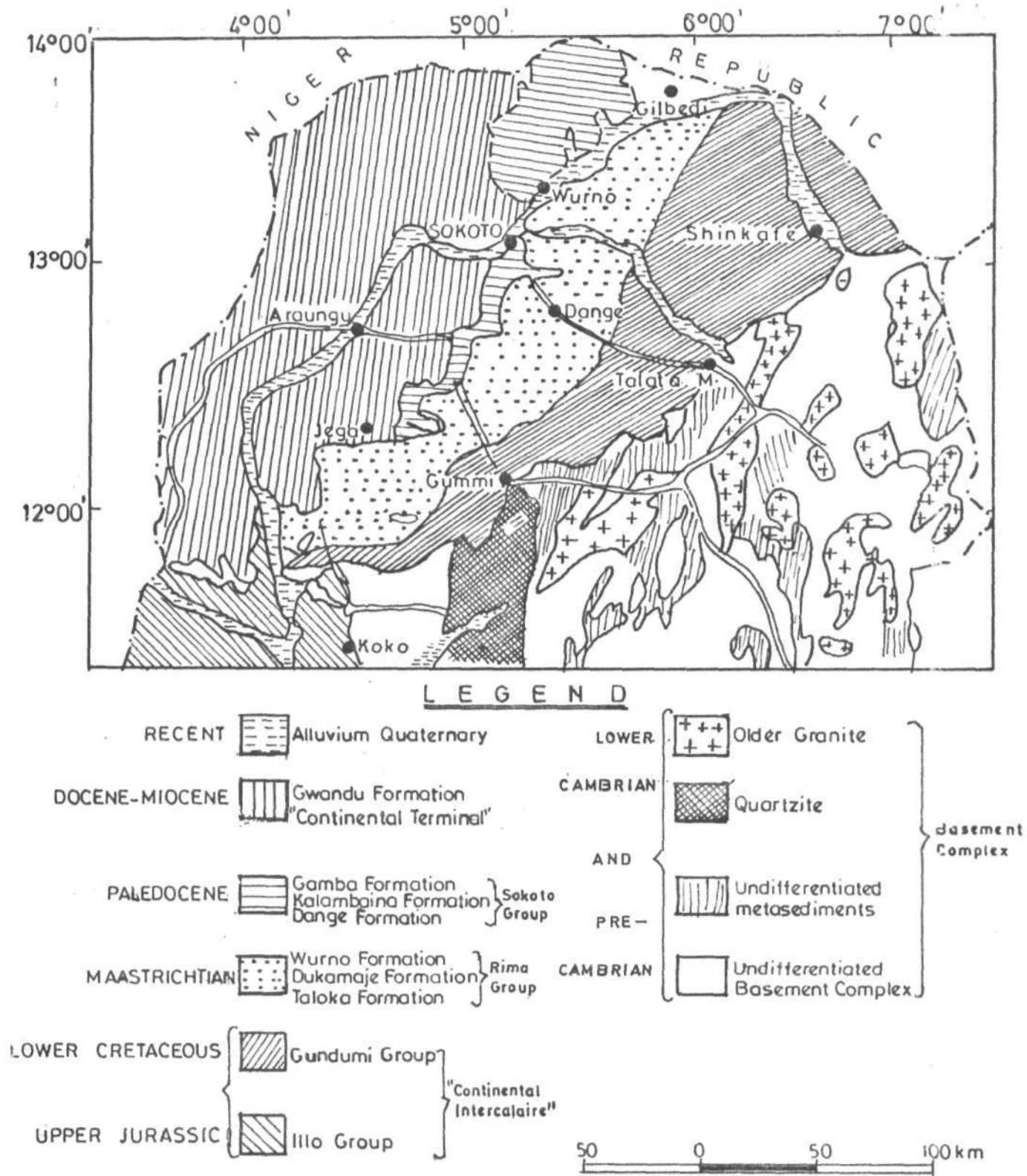
Fig·2·2: Geological map of the Sokoto Basin (After Kogbe, 1981)

Basement unconformably, the Illo and Gundumi Formations, made up the grits and clays, form part of the 'Continental Intercalaire' of West Africa. They are overlain unconformably by the Maastrichtian Rima Group, consisting of mudstones and friable sandstones (Taloka and Wurno Formations), separated by the fossiliferous shelly Daukamaje Formation. The Paleocene Dange and Gamba Formations (mainly Shales) are separated by the calcareous Kalambaina Formation. The overlying continental Gwandu Formation (Continental Terminal) is of Tertiary age.

Table 2.1 is the summary of the geological sequence in the north-western Nigerian sedimentary basin by Kogbe (1981).

2.3 THE BASEMENT COMPLEX

The entire basin is underlain by the Basement Complex which includes all rocks older than the late Proterozoic (McCury, 1976). The Nigerian Basement Complex lies within the Pan-African Mobile belt of West Africa and is believed to have a polytecto-metamorphic nature (Oyawoye, 1964; McCury, 1976; Grant, 1978) and consequent metamorphism, migmatization and gneissification have extensively modified the original rocks. Three major rock successions are distinguishable (Odeyemi, 1988) and these are:

a) polycyclic crystalline complex of migmatites and gneisses which are the dominant rocks. The evolution of this complex

Table 2.1: Geological Sequence in the Sokoto Basin
(after Kogbe, 1981).

Age	Formation	Group	Environment
Quaternary	Sandy drifts	-----	Continental
Eocene-Miocene	laterites	"Continental" Formation	Continental

---------------- U N C O N F O R M I T Y ----------------

Age	Formation	Group	Environment
Late Paleocene	Primary Oolitic ironstone		
	Gamba Formation	Sokoto Group	Marine
	Kalambaina Formation		
	Dange Formation		

---------------- U N C O N F O R M I T Y ----------------

Age	Formation	Group	Environment
Maastrichtian	Wurno Formation		brackish
	Dukamaje Formation	Rima Group	water with
	Taloka Formation		brief marine
			intercalation

---------------- U N C O N F O R M I T Y ----------------

Age	Formation	Group	Environment
Late Jurassic to earliest Cretaceous	Illo and Gundumi Formations	"Continental intercalaire"	Continental

-------------M A J O R   U N C O N F O R M I T Y --------

Age	Formation	Group	Environment
Precambrian	**Basement**	**Complex**	

is believed to have started during the Liberian Orogeny (2,800±200 Ma).

b) The metasediments and metavolcanics which form the approximately N-S trending Schist belts. The period of initiation of the sedimentary process leading to the deposition of these successions had until recently been assigned solely to the Pan African Orogeny (600±200 Ma). Recent work by Ogezi (1977), among others have indicated that part of these sediments may have formed in the Kibaran 1,100±200 Ma) times

c) The Older Granite series which belong to a suite of syn to late tectonic granite and granodiorites that marked the intrusive phase (700 - 500 Ma) of the Pan African Orogeny in Nigeria. These granitoides intrude both the migmatite-gneiss complex and the schist belts variably and are widespread in other parts of the Nigerian Basement and Pan-African province of West Africa.

2.4 THE BASIN DEPOSITS

The Illo and Gundumi Groups overlie the Precambrian basement unconformably, and are both of fluviatile and lacustrine origin. Both groups are believed to be the oldest unmetamorphosed sediments in the basin. The heavy mineral assemblage in them

indicates a high grade metamorphic origin, the source being considered to be the basement complex (Precambrian) rocks in the adjoining parts of north-western Nigeria (Kogbe, 1979).

The Illo group includes a band of pisolitic and nodular clays and contains silicified wood but is otherwise unfossiliferous. The group consists of cross-bedded pebbly grits, sandstones and clay (Jones, 1948 and Kogbe, 1981). The Gundumi groups were also unfossiliferous set of false-bedded clayey grits and clays with basal conglomerates. The clays and gritty sands represent the various changes in the dynamic conditions prevailing within the depositional environment.

The second phase in the depositional history of the Sokoto Basin sediments started during the Maastrichtian when the marine Rima group was deposited unconformably on Pre-Maastrichtian continental beds. Three formations namely Taloka, Dukamaje and Wurno Formations have been identified to belong to this group (Kogbe, 1981). Principally these formations are composed of fine grained sandstones, mudstones and clays in which is intercalated an important band of shales and limestones.

The Sokoto group (late Palaecene deposits) is made up of the Dange, Kalambaina and Gamba Formations. These formations form an outcrop band about 20 km wide near the border with Niger Republic and almost pinches out at Jega (Fig. 2.2).

The set of grits and massive white clays with sandstone and mudstone intercalations which overlies the marine Sokoto group

belong to the Gwandu group. (Kogbe, 1981 and Jones, 1948). These sediments outcrop extensively in Niger Republic and Northern Benin, where they are referred to as *"Cares du moyen Niger"* and have been correlated with sediments of Miocene-Pliocene age in Central African Republic and in Mauritania where they are known as "Continental Terminal". The non-marine origin is certain and the sediments can be attributed to a lacustrine environment (Kogbe, 1979, 1981).

The ferruginous deposits which have been subdivided into three major groups namely: ferruginous oolites, crusty-concretionary laterites and ferruginous sandstones cap the sediments over extensive areas of the basin (Kogbe, 1981). These groups of sediments whose occurrence is widespread in the Iullemmeden Basin are generally considered to be of primary origin and attain a thickness of between 3 - 5 m in Sokoto Basin area (Kogbe, 1981).

2.5 FAULTS AND FOLDS

A series of transcurrent faults have been observed to affect the basement rocks adjoining the Sokoto Basin. Wright (1968) and Ball (1980) have both identified a system of NE - SW and NW - SE conjugate pairs of fractures which exists everywhere within the Pan African Mobile Belt. It was suggested by Wright (1968) that these fracture systems represent important lines of weakness in the continental crust and could be loci of economic

mineralisation. Ball (1980) was of the opinion that this conjugate strike-slip system was due to brittle deformation during the latter part of the Pan African Orogeny. He argued that the geometry is very consistent over large areas and that this may in fact be reflecting the stress field operative during the identation of the Pan-African Mobile Belt by a more rigid West African craton. The sediments in the basin were not subjected to any remarkable degree of faulting as only some WSE-ENE trending faults have been observed in the vicinities of Dange and Gilbedi villages (Kogbe, 1981).

It was also observed that in the Sokoto Basin, the Basement Complex and its supracrustal cover of younger metasediments were subjected to two phases of tight isoclinal folding during the Pan-African which are responsible for N-S trending structures common over much of Nigeria (McCurry, 1976).

2.6 DEPOSITS OF ECONOMIC IMPORTANCE IN SOKOTO BASIN

Clays, ironstones, laterites, limestones, gypsum and gravels are the most important economic deposits in the Sokoto Basin. Others include lignite, phosphates and salts and the presence of radioactive minerals is also probable.

Limestone deposits from the Palaeocene formation around Sokoto are already being utilised for the manufacture of cement. Also gypsum, which is an essential ingredient in the manufacture of cement, occur scattered within the Dukamaje and Dange Shales.

The Rima Group of sediments is rich in gravel, lignite and salt deposits. The occurrence of lateritic and ferruginised sandstone is wide-spread throughout the basin and these have been utilized mainly for road construction purposes.

The only source of water for the inhabitants during the long (October - May) dry season is the aquifers within the basin. A zone of permanent saturation has been established to be continuous through the basin and at shallow enough depths to be reached by the local shafts (Jones 1984).

The report of the study for ground water development in Sokoto state by Japan International Cooperation Agency, JICA, (1990) shows that in the basin, sedimentary rock composed of sandstone, limestone and clay of Cretaceous to Tertiary ages forms a multilayered ground water basin. The alluvium in Fadama also contain unconfirmed groundwater. According to the result of test drilling by JICA, the pumping rate of 300 l/min is possible at a well with 100 - 150 m depth and 150 mm in diameter.

CHAPTER THREE

SPECTRAL ANALYSIS OF AEROMAGNETIC FIELDS

3.1 INTRODUCTION

Potential field data such as aeromagnetic data can be represented by one or two dimensional Fourier series consisting of various frequencies which characterize the anomalies. The amplitude and phase relationship among these frequencies constitute what is known as a "complex line spectrum" (Negi, *et al.*, 1982). This relationship has been used extensively by various workers for the interpretation of gravity and magnetic data. Bahattacharyya (1966), by Fourier-transforming the total intensity anomaly caused by a rectangular prismatic body with arbitrary polarization obtained the two dimensional spectrum of the anomaly. He found this method useful for separating the effects of near surface high-amplitude components from those of the deeper crustal sources in the total intensity map. Spector and Grant (1970), assuming a number of ensembles of rectangular sided parallelopipeds calculated power spectra from the gridded total-intensity aeromagnetic data and matched them with corresponding spectra for a theoretical model in order to determine the depth. Hahn, *et al.* (1976), by Fourier transforming the digitized aeromagnetic data over a square, computed the amplitude spectrum and plotted it on a logarithmic

scale against frequency. Their plots show straight line segments
which decrease in slope with increasing frequency. By continuing
the given field downward, these straight lines become horizontal
at a depth called "white depth". This depth is taken as estimate
for the depth of magnetic sources. In the present study, a
similar approach has been adopted.

3.2 FAST FOURIER TRANSFORM OF TWO DIMENSIONAL AEROMAGNETIC DATA

Given a residual magnetic anomaly map of dimensions L x L,
digitized at equal intervals, the residual total intensity
anomaly values can be expressed in terms of a double Fourier
series expansion:

$$T(x,y) = \sum_{m}^{N} \sum_{n}^{M} P_m^n \cos[(2\pi/L)(nx+my)] + Q_m^n \sin[(2\pi/L)(nx+my)]$$

$$....3.1$$

where L is the dimension of a block, P_m^n and Q_m^n are Fourier
amplitudes and N, M are the number of grid points along the x
and y directions respectively. The sum

$$P_m^n \cos[(2\pi/L)(nx+my)] + Q_m^n \sin[(2\pi/L)(nx+my)]$$

represents a single partial wave for which

$$\left[P_m^n \right]^2 + \left[Q_m^n \right]^2 = \left[C_m^n \right]^2$$

C_m^n is the amplitude of the partial wave; the frequency counter of the wave is given by

$$F_m^n = (n^2 + m^2)^{\frac{1}{2}}.$$

The Fourier transform of a selection of magnetic map digitised in a square grid therefore forms a rectangular matrix with coefficients which can then be reduced to a set of average amplitudes dependent only on the frequency (Hahn, *et al.*, 1976). These average amplitudes fully represent the spectrum from which the depth to the magnetic source can be estimated.

In order to represent the residual data in the above form, we have to obtain the 2-D Fourier transform of the data. This can be done by first Fourier transforming columns (or rows) and next rows (or columns). This can be shown as follows

$$\bar{x}(u,v) = \sum_{m=0}^{M} \sum_{n=0}^{N} x(m,n)\exp[-i(um+vn)]$$

$$= \sum_{m=0}^{M} [\sum_{n=0}^{N} \times (m,n)\exp(ivn)]\exp(-ium)$$

$$= \sum_{m=0}^{M} \bar{x}'(m,v)\exp(-ium) \qquad \ldots\ldots 3.2$$

where $\bar{x}(m,v)$ is a Fourier transform of mth column.

Inverse transform is obtained simply by changing the sign of i in the exponential function.

The normalised power or energy spectrum of the two-dimensional aeromagnetic data is given as follows (Naidu, 1970b).

$$s'(u,v) = 1/Mxn|x(u,v)|^2 \qquad \ldots\ldots 3.3$$

In general and for this study in particular, M = N. The number of sample points N is chosen according to relation N = 2^k for FFT analysis, where k is an integer constant.

Based on the available algorithms, the above processes have been programmed by many authors for various implementations using the binary features of a computer. For this study, an FFTDEPTH subroutine written by S. B. Ojo of Physics Department of A.B.U. Zaria (1992) was used.

3.3 DATA SOURCE

The data set used in this study was compiled from thirty half-degree aeromagnetic map sheets of GSN aeromagnetic survey series, covering the Sokoto Basin (Umego, 1990).

The digital data was obtained by digitizing the aeromagnetic maps along flight lines. The data for each sheet was gridded to generate 101 x 101 matrix. After this, the data for the entire basin was combined into a master grid comprising 707 N-S profiles with data at 0.55 km interval.

3.4 DATA TREATMENT

The use of spectral analysis to interpret aeromagnetic anomalies involved some practical problems, most of which are inherent in the application of discrete Fourier transform (DFT). These include the problems of aliasing, truncation effect or Gibb's phenomenon and problems associated with even and odd symmetries of the real and imaginary parts of the Fourier transform.

The aliasing effect arises from ambiguity in the frequency represented by the sampled data. Frequencies greater than the Nyquist frequency tend to impersonate the lower frequencies and this is known as the aliasing effect. The Nyquist frequency itself is the lowest frequency which is its own alias, that is the limit of both the sequence of frequencies and the sequence of their aliases. The Nyquist frequency also known as the folding frequency is simply given by

$$f_{nq} = \frac{1}{2}(1/\Delta x) \qquad \qquad \qquad ....3.4$$

where Δx is the sampling interval. To avoid or reduce the effects of alaising, frequency greater than Nyquist frequency must be removed through the use of an alias filter which provides high attenuation above the Nyquist frequency. Aliasing can also be reduced through the use of small sampling interval such that the Nyquist frequency is equal to or greater than the highest frequency component present in the function being analysed. The sampling interval used during the collection of data used for this work, 550 m. (0.55 km), directly imposes a Nyquist frequency of 1/1.1 km . This spacing was found adequate since we are concerned with the source originating from not more than 2 km in thickness (Umego, 1990).

When a limited portion of an aeromagnetic anomaly map is subjected to Fourier synthesis, it is difficult to reconstruct the sharp edges of the anomaly with a limited number of

frequencies and thus truncation leads to the introduction of spurious oscillations around the region of discontinuity. This is known as the Gibb's phenomenon. This truncation is equivalent to convolution of Fourier transform of the function with that of a rectangular window which is a sinc cardinal function. This convolution introduces ripples at the edges of the function, which manifests itself as spurious oscillations at the discontinuity. Increasing the length of the window makes the Fourier transform tend towards a delta function, with a subsequent reduction of the ripples at the edges. The truncation effect can therefore be reduced through the use of short sampling intervals and by selecting a large portion of anomaly or a long profile centred around the features of interest. The use of a finite data window is equivalent to applying a rectangular data window. Figure 3.1a shows the rectangular time window and the corresponding spectral window. The effect of data window in the frequency domain is to broaden the spectral lines and to introduce a series of spurious peaks called side lobes. The consequence of the presence of side lobes is that the spectral power from the adjoining frequencies leaks into and contaminates the frequency of interest. This is highly undesirable particularly in the neighbourhood of a spectral peak.

An alternative and even more effective approach to reducing the problem of Gibb's phenomena is by the application of a cosine taper to the observed data (Kanasewich, 1975). Such an

extended cosine-bell data window remains fairly flat over most of the data length therefore preserving most of the original data set but tapers off near the two ends of the records (Figure 3.1b). The tapering eliminates the high frequencies (side lobes) erroneously introduced by the sharp truncation in the rectangular data window.

A good taper consists of a pair of cosine bells. For N data points the n component is multiplied by W(t) (Figure 3.1c), where

$$W(t) = \frac{1}{2}[1 + \cos\pi \frac{(t_c - t)}{(t_c - t_m)}], \text{ for } -t_m < t < -t_c$$

$$= 1, \text{ for } -t_m \leq t \leq t_c$$

$$= \frac{1}{2}[1 + \cos\pi \frac{(t - t_c)}{(t_m - t_c)}], \text{ for } t_c < t < -t_m \qquad ....3.5$$

The procedure of smoothing the shape of the data window through the application of the cosine taper was based on the basic formulae of equation 3.5. The edges of the data array were smoothly tapered by applying the cosine taper of 15% which is equivalent to about 10 data points for the 64 x 64 data array.

3.5 THE FOURIER TRANSFORM PROCEDURE

The digitised data for the Sokoto Basin formed a square grid of a density which guarantees that all the details necessary for the given interpretation are included. The net of values is then subdivided into 116 square blocks each 34.65 x 34.65 km in

Fig.3.1a : Rectangular data window and the corresponding spectral window

Fig.3.1b : A cosine-bell data window and the corresponding spectral window

Fig.3.1c : An extended cosine-bell data window
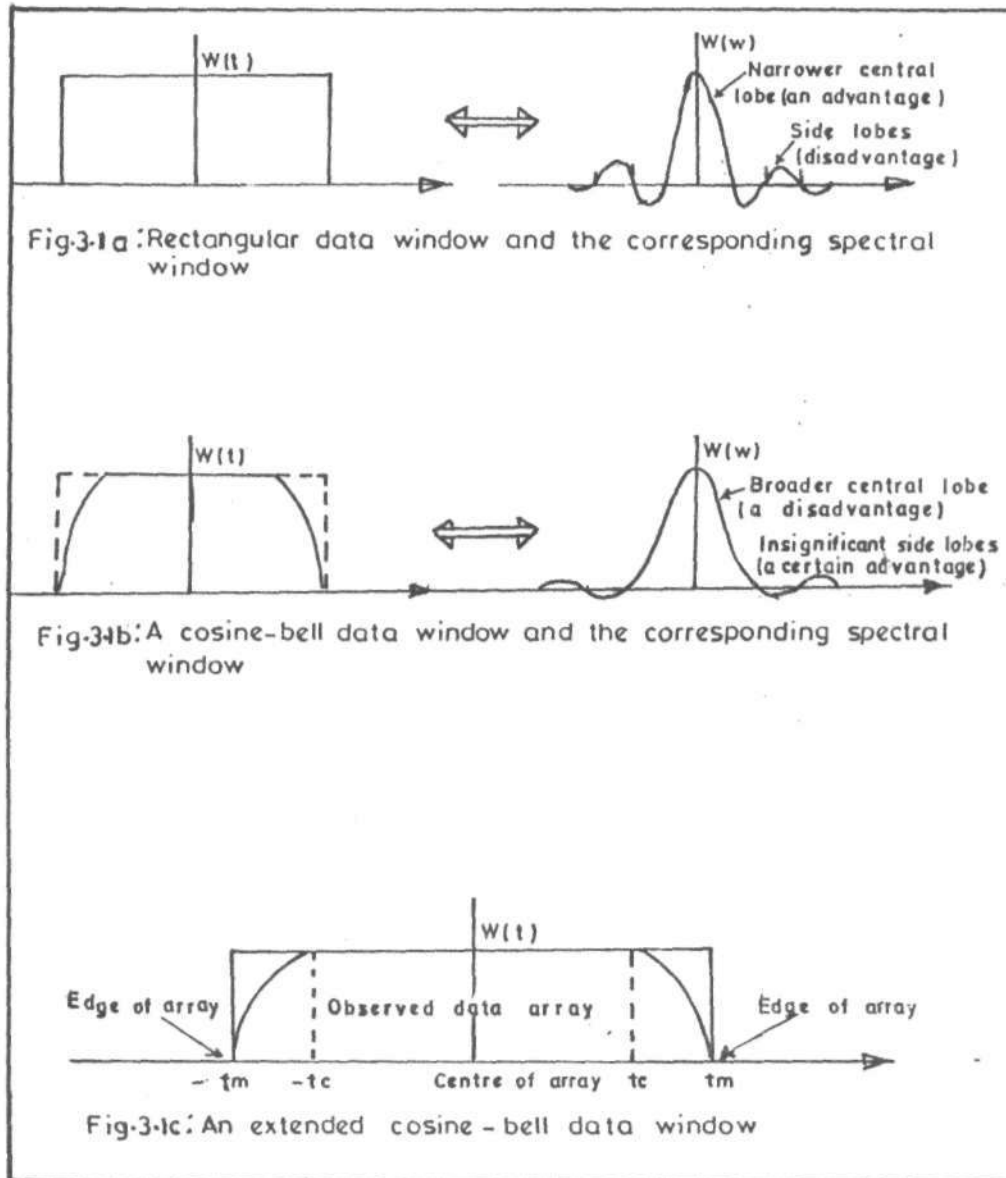
dimension, and meeting as far as possible the following conditions (Hahn, *et al*., 1976)

1) Each square contains more anomalies than one maximum-minimum pair

2) The square sides do not cut through essential parts of anomalies of single bodies.

The first condition corresponds to the fact that we consider the anomalies as a statistical population in this procedure. The second condition must be postulated because the harmonic analysis yields a set of partial waves which when resynthesized represent an artificial field which only matches the given anomalies inside the square; outside the square these anomalies are repeated like a chess-board everywhere over the plane which contains the square (Hahn, et al., 1976).

Next the two-dimensional Fourier transform of the data was computed from equation 3.2. The average amplitude spectrum of all the partial waves falling within a frequency range (0.5 of the integer in this work) was then computed by summing the Fourier amplitudes and dividing the sum by the number of frequencies. The scheme for computing the radial spectrum for map spectra is illustrated in Figure 3.2. The upper values in each block represent the normalised energy spectrum and the values below are frequencies.

	0	1	2	3	4	5	6	7	8	9	10	11	12	13	14
0	13.12 / 0	11.13 / 1	9.91 / 2	7.09 / 3	7.09 / 4	7.31 / 5	5.65 / 6	3.30 / 7	4.28 / 8	2.59 / 9	-1.25 / 10	-1.58 / 11	0.53 / 12	-0.63 / 13	-0.24 / 14
1	11.07 / 1	9.19 / 1.41	7.68 / 2.24	5.00 / 3.16	5.07 / 4.12	5.16 / 5.10	3.48 / 6.08	1.23 / 7.07	2.29 / 8.06	0.46 / 9.06	-1.51 / 10.05	-3.92 / 11.05	-1.29 / 12.0	-1.80 / 13.04	-1.25 / 14.04
2	9.88 / 2	7.66 / 2.24	6.90 / 2.83	4.28 / 3.61	3.88 / 4.47	4.17 / 5.39	2.81 / 6.32	-0.44 / 7.28	1.19 / 8.25	-0.60 / 9.22	-1.38 / 10.20	-4.15 / 11.18	-1.52 / 12.17	-2.56 / 13.15	-3.42 / 14.14
3	6.90 / 3	4.70 / 3.16	4.31 / 3.61	0.31 / 4.24	1.30 / 5.00	0.72 / 5.83	0.23 / 6.71	-0.56 / 7.62	-3.90 / 8.54	-1.67 / 9.49	-1.33 / 10.44	-1.19 / 11.40	-1.61 / 12.37	-1.34 / 13.34	-3.19 / 14.32
4	6.69 / 4	4.53 / 4.12	3.68 / 4.47	2.93 / 5.00	0.77 / 5.66	1.23 / 6.40	0.64 / 7.21	-3.35 / 8.06	-3.78 / 8.94	-1.81 / 9.85	-0.75 / 10.77	-1.50 / 11.70	-2.30 / 12.65	-1.69 / 13.60	-2.99 / 14.56
5	7.42 / 5	5.33 / 5.10	4.73 / 5.39	0.63 / 5.83	2.51 / 6.40	1.42 / 7.07	0.17 / 7.81	-0.46 / 8.60	-0.74 / 9.43	-3.70 / 10.30	-2.97 / 11.18	-1.75 / 12.08	-1.97 / 13.00	-1.13 / 13.93	-4.02 / 14.87
6	5.76 / 6	3.34 / 6.08	3.12 / 6.32	0.88 / 6.71	-2.75 / 7.21	-0.48 / 7.81	0.58 / 8.49	-1.32 / 9.22	-0.62 / 10.00	-4.13 / 10.82	-3.25 / 11.66	-1.49 / 12.53	-1.86 / 13.42	-1.14 / 14.32	-3.72 / 15.23
7	2.22 / 7	0.76 / 7.07	1.58 / 7.28	-0.92 / 7.62	0.88 / 8.06	0.89 / 8.60	-0.36 / 9.22	-2.58 / 9.90	-1.98 / 10.63	-4.18 / 11.40	-1.29 / 12.21	-0.95 / 13.04	-3.15 / 13.89	-2.50 / 14.76	2.54 / 15.65
8	4.67 / 8	1.81 / 8.06	2.70 / 8.25	1.08 / 8.54	-0.36 / 8.94	-1.31 / 9.43	-0.48 / 10.00	-2.86 / 10.63	-4.85 / 11.31	-1.16 / 12.04	-5.58 / 12.81	-1.72 / 13.60	-3.10 / 14.42	-2.92 / 15.26	-2.45 / 16.12
9	2.97 / 9	1.87 / 9.06	-2.38 / 9.22	0.65 / 9.49	-0.25 / 9.85	1.13 / 10.30	-1.47 / 10.82	-1.17 / 11.40	-3.27 / 12.04	-0.85 / 12.37	-4.63 / 13.45	-1.82 / 14.21	-1.72 / 15.00	-1.06 / 15.81	-2.05 / 16.64
10	-0.72 / 10	-1.80 / 10.05	0.40 / 10.20	-0.09 / 10.44	-1.38 / 10.77	-0.19 / 11.18	-2.37 / 11.66	-1.80 / 12.21	-1.34 / 12.81	-2.14 / 13.45	-1.97 / 14.14	-1.11 / 14.87	-2.52 / 15.62	-1.51 / 16.40	-1.17 / 17.20
11	-4.12 / 11	-0.92 / 11.05	-0.79 / 11.18	-1.31 / 11.40	-0.87 / 11.70	-2.97 / 12.08	-1.93 / 12.53	-0.54 / 13.04	-0.75 / 13.60	-3.01 / 14.21	-3.83 / 14.87	-1.92 / 15.56	-1.84 / 16.28	-1.53 / 17.03	-1.44 / 17.80
12	0.77 / 12	-0.82 / 12.04	0.61 / 12.17	-0.25 / 12.37	-2.83 / 12.65	-2.14 / 13.00	-0.64 / 13.42	-3.16 / 13.89	-1.92 / 14.42	-4.61 / 15.00	-1.83 / 15.62	-2.45 / 16.28	-3.32 / 16.97	-1.76 / 17.69	-1.50 / 18.44
13	-0.03 / 13	0.20 / 13.04	-2.16 / 13.15	-0.77 / 13.34	-4.59 / 13.60	-2.31 / 13.93	-0.57 / 14.32	-2.27 / 14.76	-0.88 / 15.26	-1.55 / 15.81	-3.31 / 16.40	-0.79 / 17.03	-1.91 / 17.69	-1.89 / 18.34	-0.80 / 19.10
14	-1.08 / 14	-0.72 / 14.04	-3.89 / 14.14	-1.18 / 14.32	-2.93 / 14.56	-0.75 / 14.87	0.02 / 15.23	-1.30 / 15.65	-2.26 / 16.12	-6.00 / 16.64	-3.32 / 17.20	-1.45 / 17.80	-2.28 / 18.44	-1.52 / 19.10	-1.49 / 19.80

LogE	13.12	10.46	8.78	6.12	4.43	4.79	2.73	0.82	1.02	-0.35	-1.07	-2.31	-1.32	-1.75	-2.04
f	.0	1.14	2.12	3.03	4.07	5.12	6.08	7.06	8.01	9.06	10.11	11.06	12.03	13.03	14.05

3.2

FIG. 3.4 : COMPUTATION OF RADIAL SPECTRUM FROM THE SPECTRUM-MATRIX

The natural logarithm of the radial spectrum for each block were then plotted against frequencies. These plots showed a series of points that may well be represented by straight lines. Most of the points due to anomalies caused by the bodies occurring within a particular depth range or at different levels fall on one or more straight line segments whose slopes provide a measure of the mean depths to the assemblage of anomalous bodies (Spector and Grant, 1970 and Hahn, *et al.*, 1976). The slope of the segments is related to the depth as follows (Spector and Grant, 1970)

$$Z = -M \qquad \qquad \qquad ....3.6$$

where Z is the mean depth of the burial of ensemble and M is the slope of the least square line. Equation 3.6 is the basic equation for the slope-depth relation for power spectrum analysis and can be applied directly if the frequency unit is in radian per kilometre. If however, the frequency unit is in cycles per kilometre the corresponding relation is expressed as

$$Z = -M/2\pi \cdot \qquad \qquad \qquad ....3.7$$

CHAPTER FOUR

ANALYSIS OF RELIABILITY OF METHOD USED WITH SYNTHETIC DATA

4.1 INTRODUCTION

Before carrying out spectral analysis and interpretation of aeromagnetic anomalies over the Sokoto Basin, tests of the procedure and computer programs to be used were carried out with some synthetic data. The primary objective of these tests was to determine the reliability and accuracy of the programs to be used in computing the sedimentary thickness of the basin.

4.2 GENERATION OF SYNTHETIC MAGNETIC FIELD FOR TEST

Three dimensional modeling of magnetic anomalies requires the analysis of data over a surface area, as well as a third dimension, depth. The vertical prism is therefore a commonly used geometric model for 3-dimensional interpretation of magnetic anomalies. Structures such as intrusive plugs and uplifted basement fault blocks can be usually approximated by prismatic models. A study of aeromagnetic contour maps suggest that most of the magnetic anomalies may be interpreted as a number of magnetized bodies which can be modelled by prismatic bodies (Bhattacharya, 1965). In general, the magnetized bodies are so close to each other that separation of the anomalies due to individual prism is not complete. Hence the contour map is

usually interpreted using multiple prisms with different magnetizations and orientations (Rao and Babu, 1991).

According to Rao and Babu (1991), the equation for the total field magnetic anomaly at any point $p(x, y, o)$ due to a vertical prism whose sides are parallel to the coordinate axes is given by

$$\Delta T(x,y,0) = G_1 \ln F_1 + G_2 \ln F_2 + G_3 \ln F_3 + G_4 F_4 + G_5 F_5 \qquad \ldots . 4.1$$

where G's are functions of the inclination and declination of geomagnetic field and those of the prisms and F's are functions of the coordinates of the field and those of the prisms.

In the course of this work, a computer program (PRISMAG) which computes the total magnetic field due to prismatic bodies was written based on the algorithm of Rao and Babu (1991) and executed on an IBM PC/AT and a CYBER 931-11 belonging to Ahmadu Bello University, Zaria (See Appendix 1A). To generate a synthetic magnetic field, a hypothetical ensemble of prisms was prepared (Fig. 4.1) with eight prisms at different locations and grouped into three different depths. The modelling program (PRISMAG) was then used to generate the total magnetic field due to these ensembles with an assumed inclination (I) and declination (D) of the prisms and those of the field. The parameters of the model field are given in Table 4.1. The field generated was machine contoured, and the results are as shown in Figure 4.2.
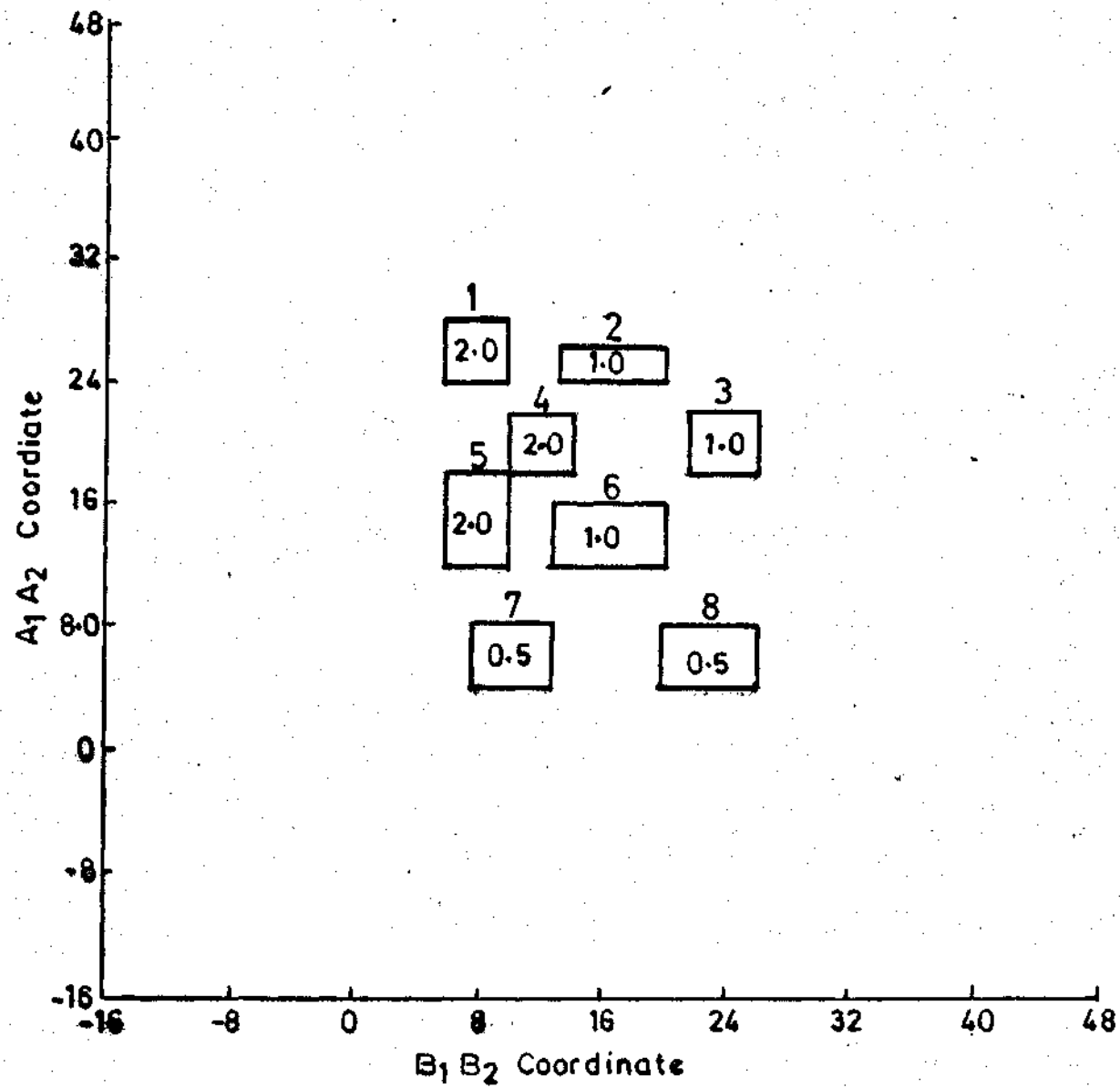
Fig. 4.1: Locations of the eight ensemble of prisms. Values in each block represent depth from the ground surface

3C

Table **4.1:** Parameters of the eight rectangular prismatic bodies

Prism No.	A_1 (km)	A_2 (km)	B_1 (km)	B_2 (km)	H_1 (km)	H_2 (km)	$I\theta$ (°)	$D\theta$ (°)	θ (°)
1	24.00	28.00	06.00	10.00	2.00	10.00	0.00	0.00	0.00
2	24.00	26.00	14.00	20.00	1.00	10.00	0.00	0.00	0.00
3	18.00	22.00	22.00	26.00	1.00	10.00	0.00	0.00	0.00
4	18.00	22.00	10.00	14.00	2.00	10.00	0.00	0.00	0.00
5	12.00	18.00	06.00	10.00	2.00	10.00	0.00	0.00	0.00
6	12.00	16.00	14.00	20.00	1.00	10.00	0.00	0.00	0.00
7	04.00	08.00	08.00	14.00	0.50	10.00	0.00	0.00	0.00
8	04.00	08.00	20.00	26.00	0.50	10.00	0.00	0.00	0.00
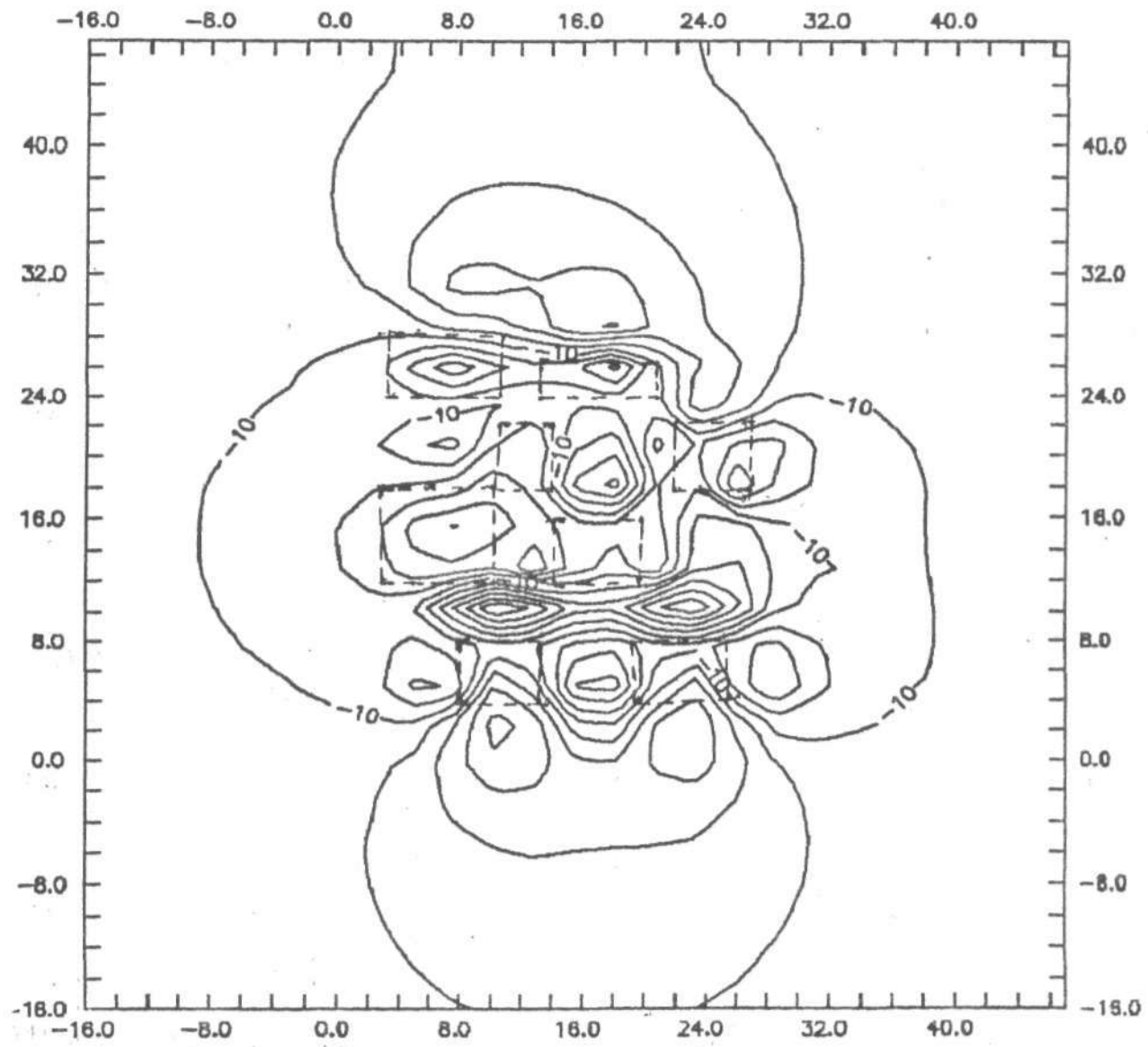
Fig.4.2 : Synthetic Magnetic contour map of the eight prismatic bodies

The field parameters are as follows:

Inclination (I) = -4.5°

Declination (D) = 0.0°

Magnetic field strength (T) = 32500 nT

and

Magnetic Susceptibility (CGSK) = 0.00385

4.3 SPECTRAL PREDICTION OF SOURCE DEPTHS FROM SYNTHETIC MAGNETIC FIELD

The application of spectral analysis to the interpretation of aeromagnetic anomalies is now sufficiently well established (Bhattacharyya, 1966; Spector and Grant, 1970; Mishra and Naidu, 1974 and Hahn, *et al.*, 1976). The method allows an estimate of the depth of an ensemble of magnetized blocks of varying depths, widths, thickness and magnetizations. Most of the approaches used involve Fourier transformation of digitised aeromagnetic data to compute the energy (or amplitude) spectrum. Two examples are presented in this study to test the reliability of the various procedures employed and hence to demonstrate the efficacy of the spectral approach. The synthetic magnetic data used in these test examples were generated as described in the previous section. These anomalies were caused by simple three-dimensional models representing common geological forms (see Figure 4.1).

With the first model of eight prisms three of the structures are located at a uniform depth of 2.0 km, another three at a depth of 1.0 km, while the remaining two are located at a depth

of 0.5 km (Table 4.1). Sampling interval of the data is 0.5 km and block size of 64 x 64 data points.

By applying the Fast Fourier transform methods using the FFTDEPTH program (Ojo, 1986) a two dimensional energy spectrum of the total magnetic field intensity anomaly over the models was computed and analysed. Figure 4.3 shows the radial spectral plot for the model field shown in Figure 4.1. The straight line segments on the plots were fitted by least squares. The correlation between the chosen depths of the models and the values of the corresponding depths obtained using the FFTDEPTH program are displayed in Table 4.2. The results show a good performance of the program at the shallower sources of 0.5 km and 1.0 km with relative percentage error of 6% and 3% respectively. It was, however, observed that the deeper sources of 2.0 km were not accurately estimated by the program with this data spacing and block size of 32 x 32 km.

Additional tests were carried out to improve the depth prediction capability of the program for deeper sources. For this, the block size was increased to 64 x 64 km. However, because of memory constraints of the computers used, it was not possible to maintain the data spacing of 0.5 km and a spacing of 1.0 km was used. Figure 4.4 shows the radial spectral plot obtained when the FFTDEPTH program was used to compute the energy spectrum of the total magnetic field intensity over the model field. Table 4.3 shows the correlation between the true model value of the depths and the value obtained using the
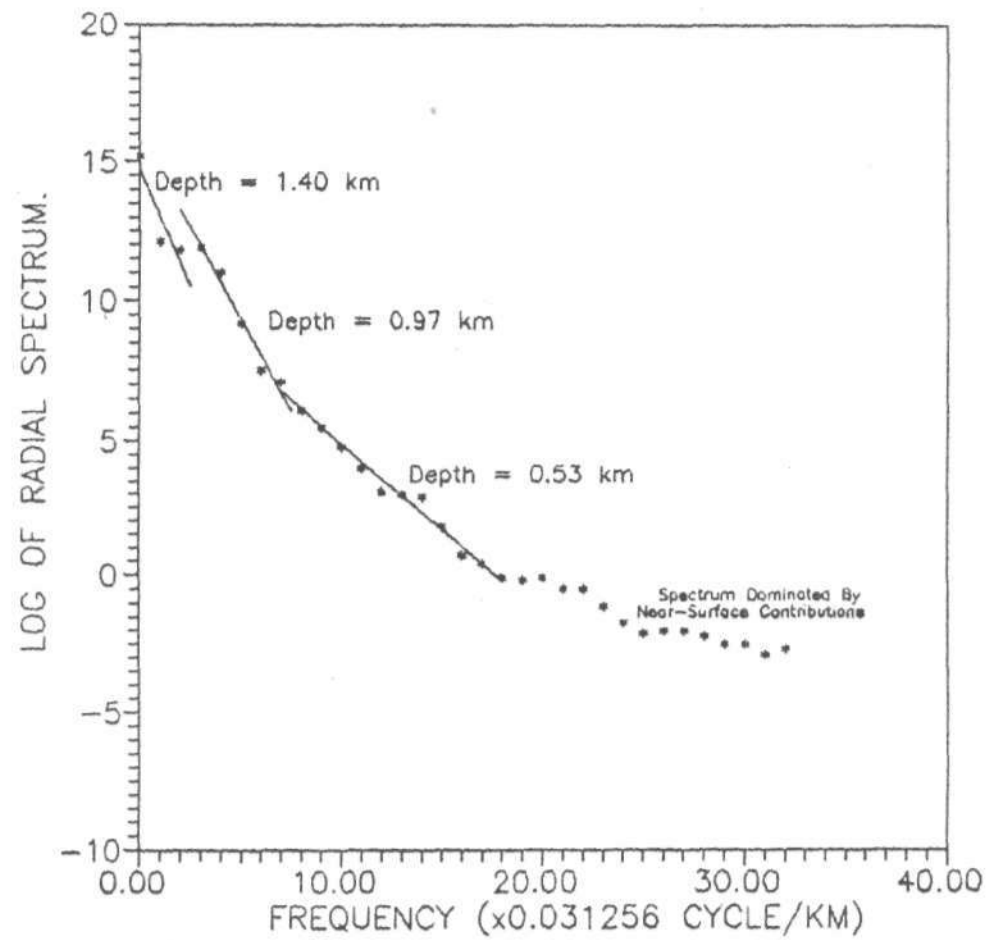
Fig.4.3: Power Spectrum Analysis For Synthetic Data
Obtained Using 8-Prism Ensemble for 0.5 km
Spacing.
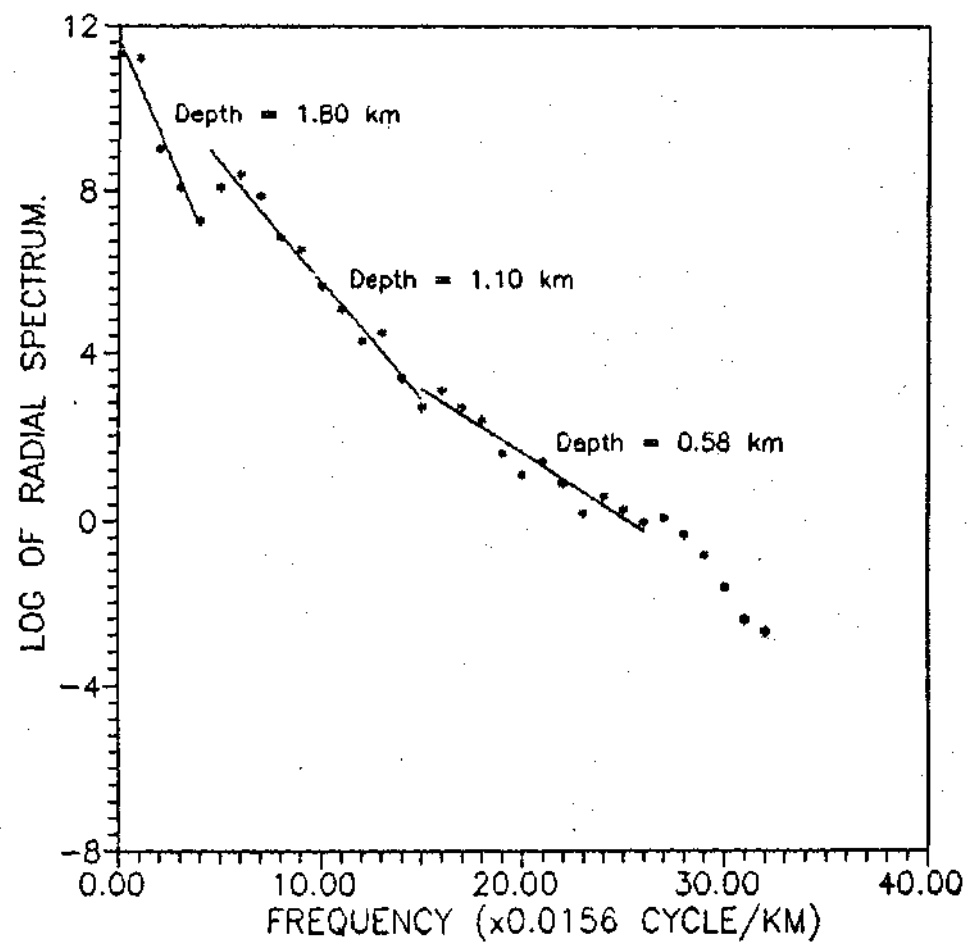
Fig.4.4: Power Spectrum Analysis For Synthetic Data
Obtained Using 8—Prism Ensemble for 1.0 km
Spacing.

Table 4.2: Depth estimates with 0.5 km data spacing and 64 x 64 points

DEPTH SEGMENT	TRUE DEPTH (km)	VALUES OBTAINED FROM FFTDEPTH PROGRAM (km)	RELATVE ERROR (%)
1st Segment	2.00	1.40	30.00
2nd Segment	1.00	0.97	3.00
3rd Segment	0.50	0.53	6.00

computer program. With a block size of 64 x 64 km, the results now show satisfactory performance of the program at the deeper (2 km) sources. The results of these tests informed the use of different block sizes depending on the depth range of interest. Thus for the data sizes of 64 x 64 points used, two data spacing of 0.55 km and 1.10 km were used in the analysis of real data in this study, with the expectation that the shallower sources will be accurately resolved using 0.55 km spacing while the deeper sources will be better estimated with 1.10 km spacing.

Table 4.3: Depth estimates with 1.0 km data spacing and 64 x 64 points

DEPTH SEGMENT	TRUE DEPTH (km)	VALUES OBTAINED FROM FFTDEPTH PROGRAM (km)	RELATVE ERROR (%)
1st Segment	2.00	1.80	10.00
2nd Segment	1.00	1.10	10.00
3rd Segment	0.50	0.58	16.00

CHAPTER FIVE

DATA ANALYSIS, RESULTS AND INTERPRETATION

5.1 INTRODUCTION

The ultimate objective of magnetic interpretation is to deduce the geometry of magnetic bodies causing a given set of anomalies. Unfortunately, however, an infinite number of sub-surface distribution of magnetizations can, in principle, be found to explain a set of magnetic field observations on the earth's surface. Normally, therefore, interpretation of aeromagnetic data have been divided into three main groups:

a) Qualitative method:- Study of maps.

b) Profile method:- Involving inspection of profiles

c) Map analysis:- deals with mathematical processes applied to map data (Reford and Sumner, 1964).

Qualitative interpretation technique may be regarded as a fine art; the experienced interpreter can usually see geologic structures merely by looking at a magnetic map, much as one can visualize surface features from the contours of topographic map. Frequently there is a connection between magnetics and topography in mineral exploration are (Telford, et al., 1976).

The more effective quantitative methods of data treatment are applied whenever it is more important to extract definite

parameters from magnetic data. Basement depths are needed in oil surveys for example, while in mineral surveys susceptibilities and dips are more important. Mathematical expressions are often employed to solve the problem of determining these parameters using profile methods. The use of residual maps, second vertical derivatives and upward and downward continuation interpretation techniques can be grouped as the map method. This method is capable of yielding information on depths to the top of causative bodies as well as emphasize special attributes of the total field map.

5.2 QUALITATIVE DESCRIPTION OF THE ANOMALIES AND DISCUSSION OF TRENDS

Figure 5.1 shows the composite magnetic-anomaly map of Sokoto Basin as prepared by Umego (1990). The (primary) data set used in preparing the map were in the form of aeromagnetic maps. Thirty 1:100,000 aeromagnetic maps published in half degree sheets were compiled to produce a master map of the field over the study area. The dynamic range of the total intensity magnetic field is 700 nT, the contour levels ranging from 7385nT to 8085 T with an average value of 7820 nT.

A quick look at the composite magnetic-anomaly maps shows that the field is characterized by a complicated pattern of high and low frequency anomalies which are circularly or elliptically shaped. A careful study of the map reveals a complex pattern of

COMPOSITE MAGNETIC-ANOMALY MAP OF SOKOTO BASIN
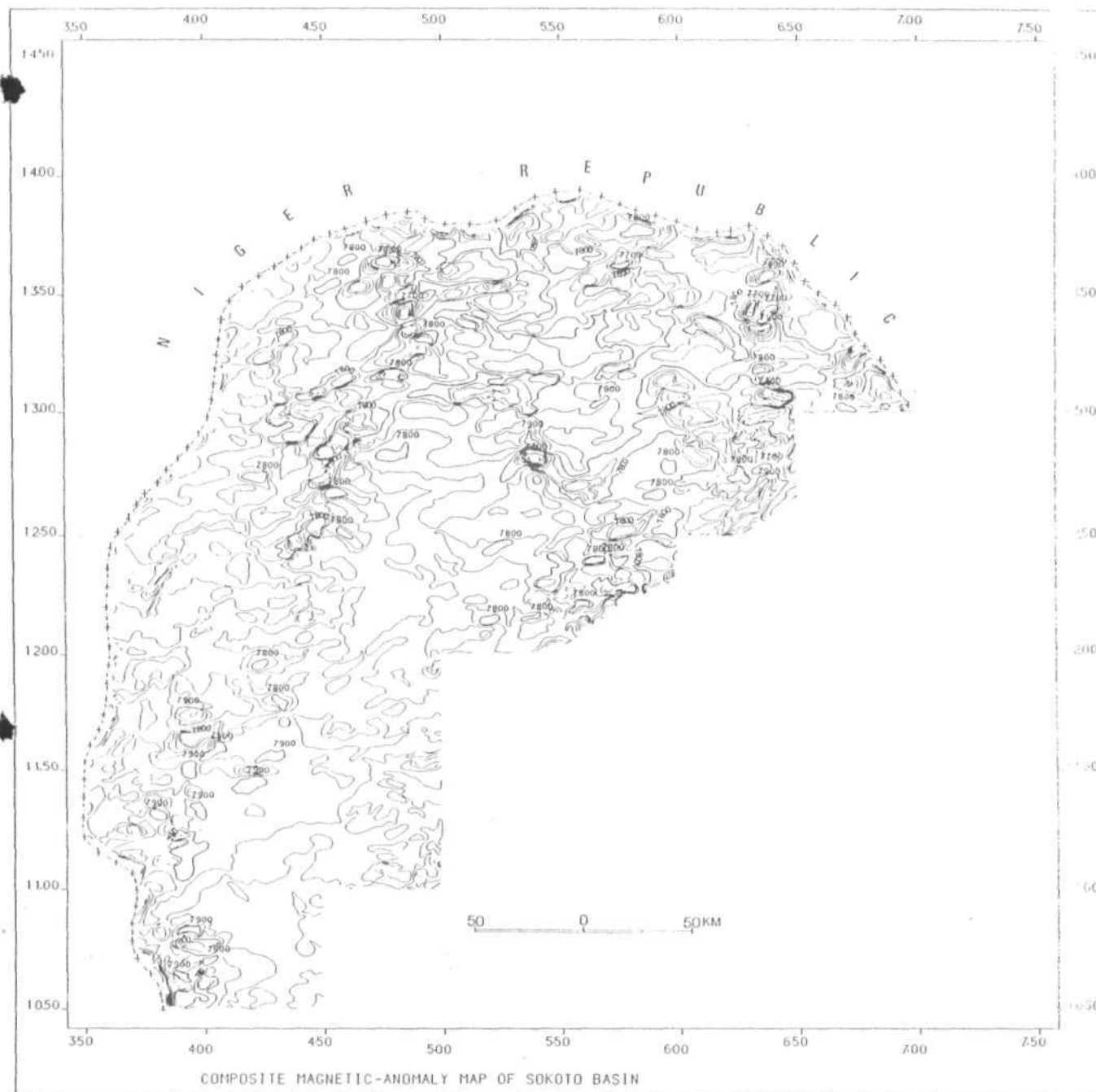
Fig. 5.1   Total magnetic field intensity contour map of Sokoto
Basin. Contour interval is 20 nT. Field values are
relative to a 25,000 nT base. (Photo - reduction
of map compiled at a scale of 1:900,000), (After
Umego 1990).

high frequency anomalies in three different locations of the study area (Umego, 1990). These are:

a) the (dominant) NNE - SSW trend which continues for some kilometres, extending from latitude 13.75°N and longitude 4.60°E to latitude 10.50° N and longitude 3.85°E.

b) the NW-SE trend in the northern part of the study area, which extends from latitude 13.75° and longitude 4.50° to latitude 12.25° and longitude 5.80°.

c) the N-S trend also in the northern part of the study area which extends from latitude 13.75° and longitude 6.45° to latitude 12.5° and longitude 6.40°.

The shape of these high frequency anomalies is suggestive of shallow intrusives either within the sediments or on the underlying basement surface. These three trends of high frequency anomalies were described as three sets of magnetic lineations (Umego, 1990).

The southeastern part of the basin and other regions outside the linear belts are characterised by low frequency anomalies with low gradients which is suggestive of either a deeper source horizon or uniform magnetic properties of the underlying basement rock.

5.3 CORRELATION BETWEEN THE MAGNETIC ANOMALIES AND SURFACE GEOLOGICAL INFORMATION

One of the most useful geological application of magnetic surveys is the mapping of structural trends by following lineations in magnetic contours. In some cases the lineations reflect the strike lines of elongated intrusive features or surfaces of large faults reflected in the basement topography or lithology (Dobrin, 1976).

It should be noted that the composite magnetic anomaly map was compiled from a digitized data sampled on a 1.1 km grid (Umego, 1990). The implications of this sampling interval is that the narrowest features that can be accurately defined by this map has a width of about 2.2 km. Also, some of the geological boundaries on the geology map of the study area are only approximate. Therefore, correlation between the two maps may be affected by these limitations.

A critical study of the Figures, 5.1 and 2.2 show that some of the prominent features of the magnetic field anomalies correlate fairly well with the surface geological information. Part of the area overlain by the Gwandu formation of Eocene-Miocene age on the geological map have on the composite magnetic-anomaly map, intense magnetic anomalies with a dominant NNE-SSW trend concentrated over them. The Gwandu formation (continental terminal) itself, is covered by a thick layer of ferruginous sandstone and lateritic crust. This lateritic crust

which is most probably of Quaternary age also overlies most of the Pre-Maastrichtian sediments making up the Illo and Gundumi group on the geological map.

Another important feature evident on the composite magnetic-anomaly map which is however not matched by any apparent surface geological feature is the nearly circularly shaped anomaly near Dange village. This anomaly with its high gradient is situated in an area where there exists the lower sandstones and mudstones of the Rima Group with a maximum thickness of about 100 metres (Kogbe, 1981). The remaining part between Talata Mafara and Koko area are characterised by low frequency anomalies with no regular shape. These anomalies with general trend in the NE - SW direction may be attributed to deep lying basement corresponding to thick lower Cretaceous sediment in the east and undifferentiated metasediment in the west.

5.4 RESIDUAL-REGIONAL SEPARATION

The critical phase in the interpretation of magnetic anomalies which is also the most sensitive source of error in the final interpretation is the separation of regional anomalies from the total magnetic anomalies to obtain the residual anomalies. The terms "residual" and "regional" are commonly used to differentiate between anomalies from local, near surface masses and those arising from larger and generally deeper fractures, respectively. The regional anomalies are usually of

long wavelength, and show a gradual change in value while the residual anomalies may show large variations over a short distance. In many cases, the choice of regional depends on the residual anomalies targeted for interpretation. There are many methods developed to separate the regional from the magnetic field or residual from the total field. The most extensively used methods are enumerated below.

5.4.1 METHODS OF RESIDUAL - REGIONAL SEPARATION

Graphical Method

This is the earliest method for estimating the regional effect by means of smooth curves on profiles or smooth contours on maps. This method is slow and cannot be automated. The only constraint imposed on the regional field, besides the interpreter's intuition, is the smoothness. As a result, there will be several solutions to the separation problem, and the inherent subjectivity may be either an advantage or a drawback depending on the interpreter's experience and ability to incorporate relevant geologic information about the regional field.

Grid (Spatial Domain) Method

In an effort to minimize the ambiguity and subjectivity entailed by the graphical method, in addition to the very considerable labour required by experienced personnel, the grid methods were developed. The procedure is really a simple way of removing the regional by second derivative analysis. The regional is considered to be the average value in the vicinity of the station, and is obtained by averaging observed values on the circumference of a circle centred at the station. The result obtained depends on the choice of the number of points on the circle and particularly on the radius selected. Clearly, if the radius is very small the residual will be zero, if it is too large the residual is approximately the station's value. Also relatively large circles may overlap other nearby residuals which would make the result meaningless.

Spectral Method

This method on the other hand provides more quantitative means to characterize the smoothness of a regional field, namely by its predominantly low-frequency spectral content. It is faster and less subjective than the graphical method because the separation is performed by filtering the total field with a suitable low-pass filter. In applying the spectral

method, regional fields may be assumed to be produced either by wide or deep-seated sources. However, due to the overlap of the regional and residual spectra, a complete separation is not possible and two kinds of errors, signal distortion and noise transmission, are always present.

Polynomial Fitting Method

This method assumes that a polynomial surface adequately models the regional field whose smoothness is controlled by the polynomial order. In this method, a least square operation is carried out which determines the potential 'surface' that fits a given observed magnetic map. The closeness of the fit depends on the degree or order of the calculation. One of the basic assumptions in its application is that the regional is a relatively low order effect, i.e over the area being analysed the true regional could be well approximated by a low order polynomial while other anomalies cannot.

5.4.2   THE REGIONAL FIELD OF THE SOKOTO BASIN.

In order to separate the regional trend from the total intensity field, a polynomial of first degree was fitted to the aeromagnetic data using the least square techniques. Krumbein (1959) showed that the equation of a linear surface may be represented by

$$Y(1) = a + bU + cV \qquad\qquad ....5.1$$

where $Y(1)$ is computed value of the linear surface at the point (U,V) and a, b and c are the linear coefficients. The deviation from the linear surface $[X_{ij} - Y(1)_{ij}]$ represents the true residual plus the trend component higher than linear.

Based on an algorithm developed by Krumbein (1959) a computer program that computes the coefficients a, b and c was written during the course of this study. These coefficients were then used to calculate $Y(1)$ for the linear surface at the control points on the maps. With these coefficients, the expression for the regional surface over the study area was found to be given by:

$$Y(1) = 8234.1 - 31.787U - 20.469V \qquad\qquad ....5.2$$

where U (the north - south coordinate) and V (the east-west coordinate) are the grid coordinates in degrees. They describe the position of the data points with respect to the origin of the two axes of the data array.

Equation 5.2 was then used to obtain the regional contour map of the Sokoto basin as shown in Figure 5.2. The regional map
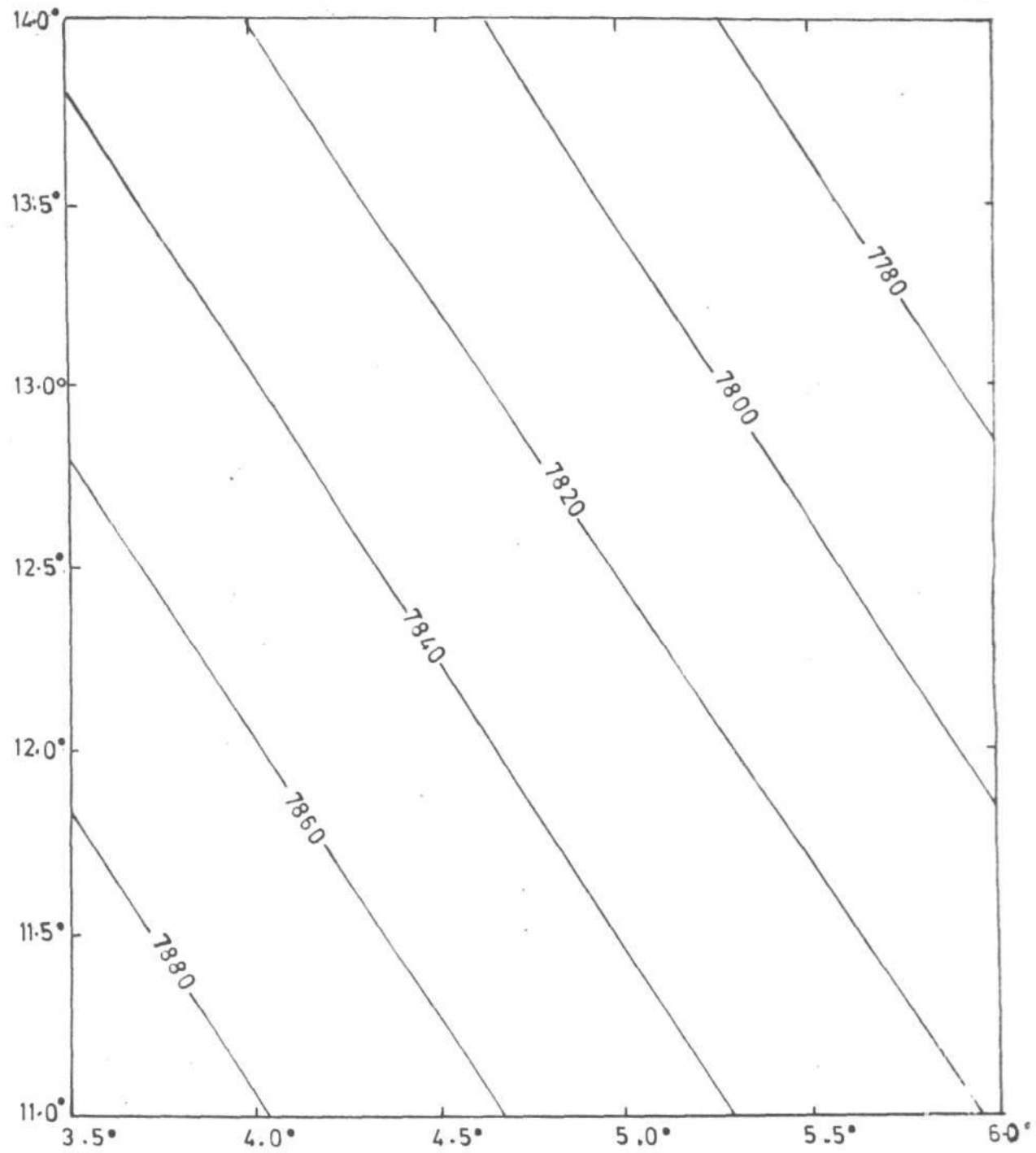
Fig.5.2. Regional magnetic field of the survey area derived from first order polynomial surface fit to the aeromagnetic data. A value of 25,000 nT must be added to values to obtain the true total field values.

which is the smooth part and is attributed to the effects which are too deep or too broad or too great in relief to be possible expression of structures or disturbances of interest has a NW-SE trend. The regional trend was subtracted from the original (observed aeromagnetic) data to obtain residual anomalies. These residual anomalies contain the components of the field which presumably are caused by the geological disturbances of interest.

5.5 QUANTITATIVE INTERPRETATION

There are various effective methods of interpreting potential field data quantitatively. One of these is the map method. The maps have the advantage of presenting the total picture available without any assumption regarding strike and lateral extent of the source (Jain, 1976). Aeromagnetic maps are used extensively in exploration for petroleum for the primary purpose of calculating the thickness of the sedimentary section. The underlying rock is referred to as 'basement', and aeromagnetic data are generally effective in determining this basement-sedimentary interface because the basement ordinarily has much larger magnetic polarization than sedimentary rock (Vacquier, *et al.*, 1951).

5.5.1 RELATIONSHIP BETWEEN MAP SIZES AND TARGET DEPTHS

The use of a finite data window is practically inevitable in two dimensional spectral analysis. Since we must limit ourselves to data of finite length or area, the target depth of interest invariably is a factor in determining the size of map or data length to be used in the analysis. Analysis of a large map size has an edge over the smaller ones because one can conveniently investigate deeper magnetic sources possibly down to the Curie surface (Naidu, 1970a). The minimum map size to be analysed is of the order of 40 to 50 times the target depth (Naidu, 1970b). Using this relationship as a rough guide and bearing in mind the results of the tests in chapter four and the estimated maximum sedimentary thickness in the Sokoto Basin of 2.00 km (Umego, 1990), two map windows were chosen and analysed. The map windows are as follows:

i)   116 blocks of approximately 35 km x 35 km map size

ii) 29 blocks of approximately 55 km x 55 km map size (or $\frac{1}{2}°x\frac{1}{2}°$).

Each of the blocks of size 35 km x 35 km consists of 64 x 64 data points sampled at 0.55 km interval. The bigger blocks of 55 km x 55 km consists of 101 x 101 data points. However, in order to satisfy the Fast Fourier Transform (FFT) requirements of 2^k points, these blocks were padded by adding 27 zeros to both the

rows and columns of each block to give 128 x 128 data points. For the FFT analysis however, every other point, corresponding to a sampling interval of 1.1 km was utilised because of the memory limitations of the computer used.

Since the block sides must not cut through the essential part of the anomalies of single bodies (Hahn, *et al.*, 1976), efforts were made when this happened to combine the adjoining sections of maps with the anomalies at the centre. Thus there was a third set of combined blocks which is made up of five blocks of 55 km x 55 km map size each.

As discussed in section 4.3, the depth results estimated from the spectral plots of 1.0 km data spacing (63 km x 63 km map size) are more accurate for deeper sources while the results with 0.5 km data spacing (31.5 km x 31.5 km map size) are more accurate for the shallower sources. Thus, in the final determination, the smaller sized blocks were used for the shallower depths of up to 1.0 km, while the larger blocks were used to determine depths exceeding 1.0 km. It is important to note at this juncture that spectral depths are in general, average depths and individual depth estimates may have values which differ from these depths.

5.5.2   ENERGY SPECTRUM ANALYSIS FOR 35 km x 35 km BLOCKS

The grid locations for the $\frac{1}{2}°$ x $\frac{1}{2}°$ aeromagnetic maps which cover the project area is shown in Figure 5.3, and examples of

some of the spectral plots for the 35 km x 35 km map size are presented in Figures 5.4, 5.5 and 5.6. Most of the energy spectra show more than one straight line segment with a different slope for each segment. A spectrum with two or more such segments normally indicates an arrangement of magnetic sources which occur at two or more different depths. On the measuring plane, each of these layers of magnetic sources would alone produce a linear spectrum (Hahn, *et al.*, 1976). It must be noted that where only two straight line segments with different gradients occur, they may not necessarily be produced by an arrangement of magnetic sources at two different depths. It might also be possible that only the segment with steeper gradient is due to magnetic source whereas the gentle sloping segment may be the expression of some noise which is not completely random, but shows some degree of auto-correlation (Hahn, *et al.*, 1976). Such noise can be introduced into the data by the smoothening procedure which in almost all cases, takes place between measuring and digitizing the data for interpretation.

It should be observed from Figure 5.3 that blocks 31, 51, 52, 73 and 96 lie very close to the basement complex area while blocks 1, 2, 3, 4, 5 and 8 are situated near the Nigerian boader with Niger Republic. The energy spectrum of these blocks (for example, Figures 5.7, 5.8 and 5.9) show what Hahn (1976) described as a white tail. This white tail signals the noise level or the high frequency end of the spectra dominated by near
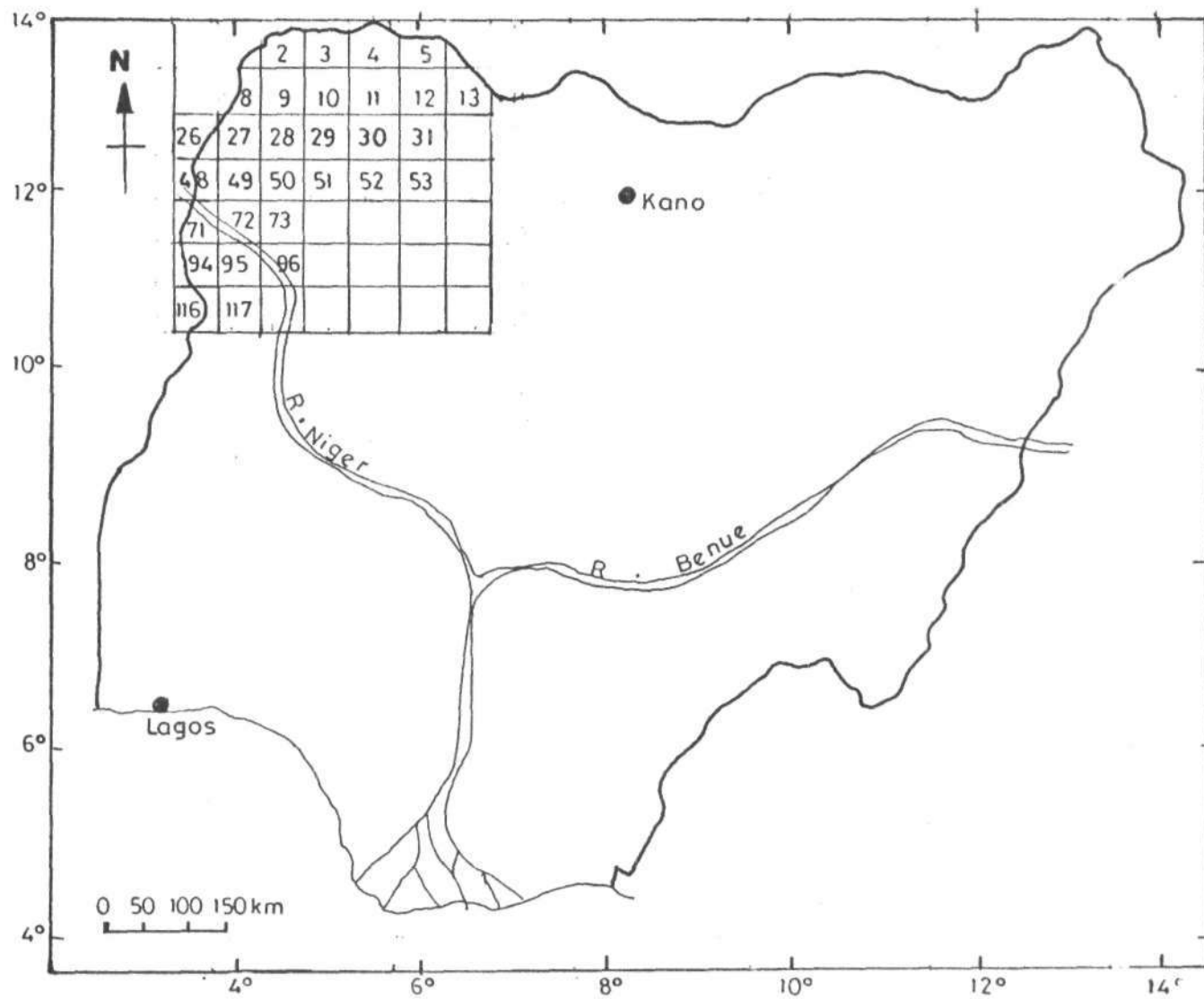
Fig.5.3 Grid locations for $\frac{1}{2}° \times \frac{1}{2}°$ blocks

Fig. 5.4: Power Spectrum Analysis For Block 48B

Fig. 5·5 : Power Spectrum Analysis For Block 49B

Fig. 5·6: Power Spectrum Analysis For Block 49C

Fig. **5·7**: Power Spectrum Analysis For Block 52D

Fig. 5·8:: Power Spectrum Analysis For Block 4A

Fig. **5.9** : Power Spectrum Analysis For Block 31D

surface contributions due to shallow basement. The latter is more probable in this case.

A summary of the spectral depths for each of the 116 blocks of 35 km x 35 km size are shown in Figure 5.10. The map sheet number are indicated at the top of each block, while the four quadrants of the sheets (a, b, c, d) are separated by dashed lines. Within each quadrant the depth values for the different segments of the energy spectra are given in increasing order of magnitude after subtracting the nominal flight elevation of 150 metres.

5.5.3 CORRELATION BETWEEN 55 km x 55 km MAP SIZE AND 35 km x 35 km MAP SIZE

Figure 5.11, 5.12, 5.13 and 5.14 present the energy spectrum for four selected blocks of 55 km x 55 km map size. As for the case with the 35 km x 35 km map size, the spectral plots of blocks close to the basement complex area show that the high frequency end of the plots is dominated by near surface contribution (for example Figure 5.14). A summary of the spectral depth estimates for the 29 blocks of these bigger map sizes are shown in figure 5.15. The first figure in each block identifies the map sheet number while the second and the third Figures refer to the shallow and deep source depths respectively after subtracting the nominal flight elevation. There are no

4°   5°   6°

1		2		3		4		5	
–	–	0·12	0·41	0·12	–	–	–	–	0·05
0·00	0·55	0·86	1·45	0·63	0·23	0·36	0·35	0·33	0·70
0·45	0·08	0·17	0·11	0·26	0·34	0·21	0·25	–	–
0·86	0·45	0·65	0·60	0·71	0·45	0·38	0·65	0·28	0·42

8		9		10		11		12	
0·00	0·13	0·16	0·24	0·11	0·11	0·00	0·16	0·09	0·31
0·53	0·63	0·53	0·58	0·80	0·55	0·74	0·63	0·53	0·68
0·17	0·14	0·10	0·18	0·25	0·24	0·23	0·16	0·10	0·17
0·64	0·53	0·64	0·56	0·40	0·36	0·53	0·57	0·31	1·15

13°

26		27		28		29		30		31	
–	–	0·02	0·05	0·30	0·15	0·08	0·00	0·13	0·10	0·08	0·04
0·31	0·17	0·51	0·33	0·58	0·68	0·44	0·19	0·49	0·69	0·10	0·29
–						1·40	0·85	–	–	0·95	
0·29	–	0·29	0·05	0·08	0·11	0·00	0·05	–	–	0·02	–
0·79	0·36	0·46	0·42	0·12	0·42	0·18	0·39	0·04	0·13	0·16	0·06
–	–	0·95	–	–	–	0·85	1·25	0·29	0·57	0·61	0·85

48		49		50		51		52	
–	0·11	0·08	0·12	0·18	0·15	0·12	0·13	0·08	0·05
0·40	0·52	0·30	0·35	0·69	0·49	0·46	0·38	0·40	0·28
–	–	0·67	–	–	–	–	–		
–	0·12	0·09	0·08	0·12	0·08	0·06	0·00	–	0·00
0·44	0·41	0·24	0·35	0·45	0·71	0·66	0·13	0·13	0·30
–	–	0·79	–	0·81	–	–	0·63	–	–

12°

71		72		73	
0·25	0·14	0·00	0·05	0·03	0·15
0·69	0·62	0·30	0·71	0·29	0·30
–	–	0·80	–	–	–
–	–	–	0·00	–	–
0·40	0·11	0·10	0·14	0·08	0·06
–	0·79	0·63	0·85	1·35	0·56

94		95		96	
0·07	0·05	0·28	0·05	0·03	0·07
0·38	0·17	0·40	0·26	0·58	0·28
–	0·42	0·66	0·85	–	–
0·05	0·00	0·01	0·03	0·07	0·00
0·16	0·13	0·22	0·28	0·67	0·59
0·40	0·31	0·76	0·72	–	–

11°

116		117	
–	–	0·05	0·16
0·32	0·41	0·53	0·85
0·03	0·00	0·00	0·28
0·40	0·58	0·49	0·85
–	–	–	–

Fig. 5·10: Summary of the spectral depths for the blocks of 35km x 35km size. The map sheet number are indicated at the top of each block and the fou:

Fig. 5·11 : Power Spectrum Analysis For Block 49

Fig. **5·12** : Power Spectrum Analysis For Block 95
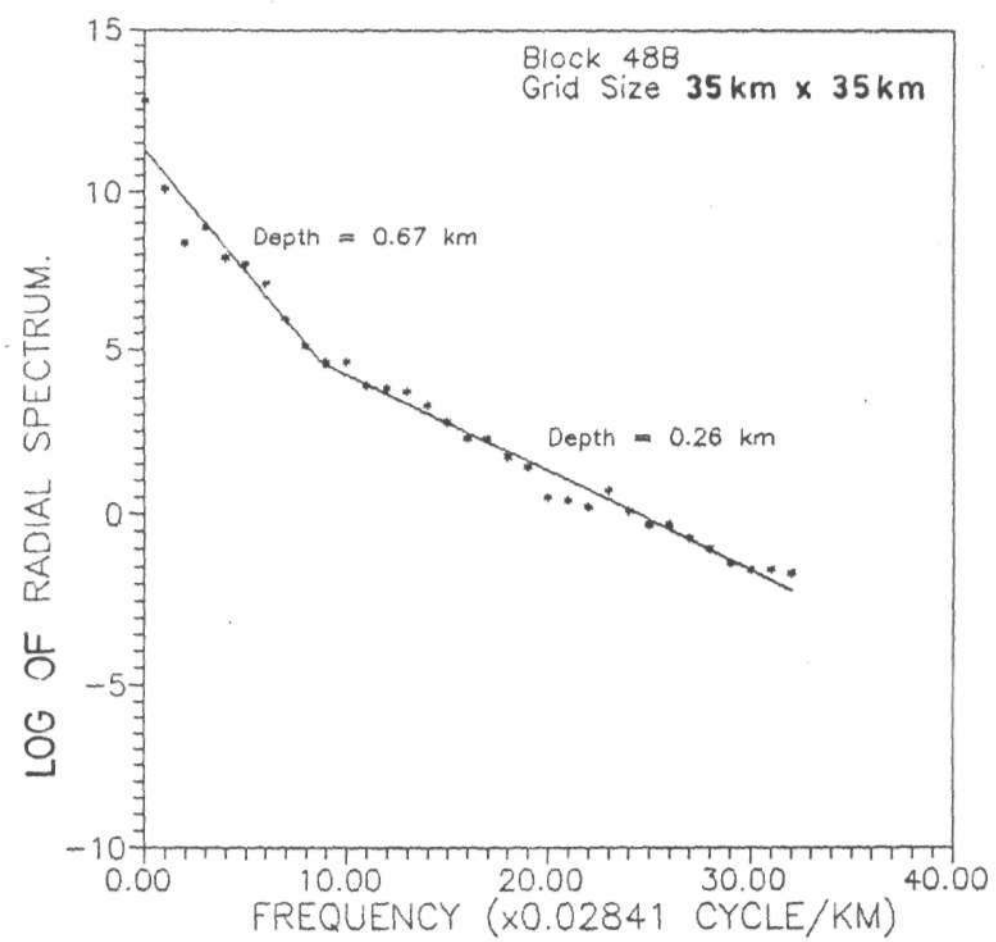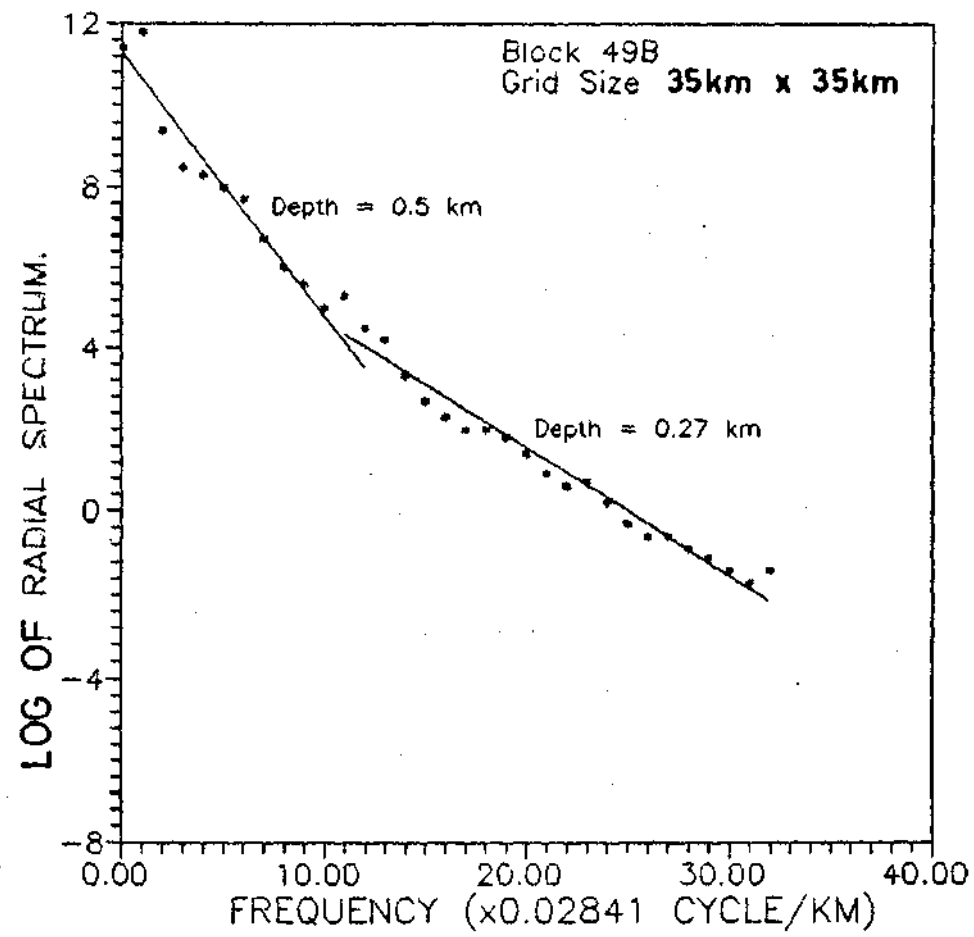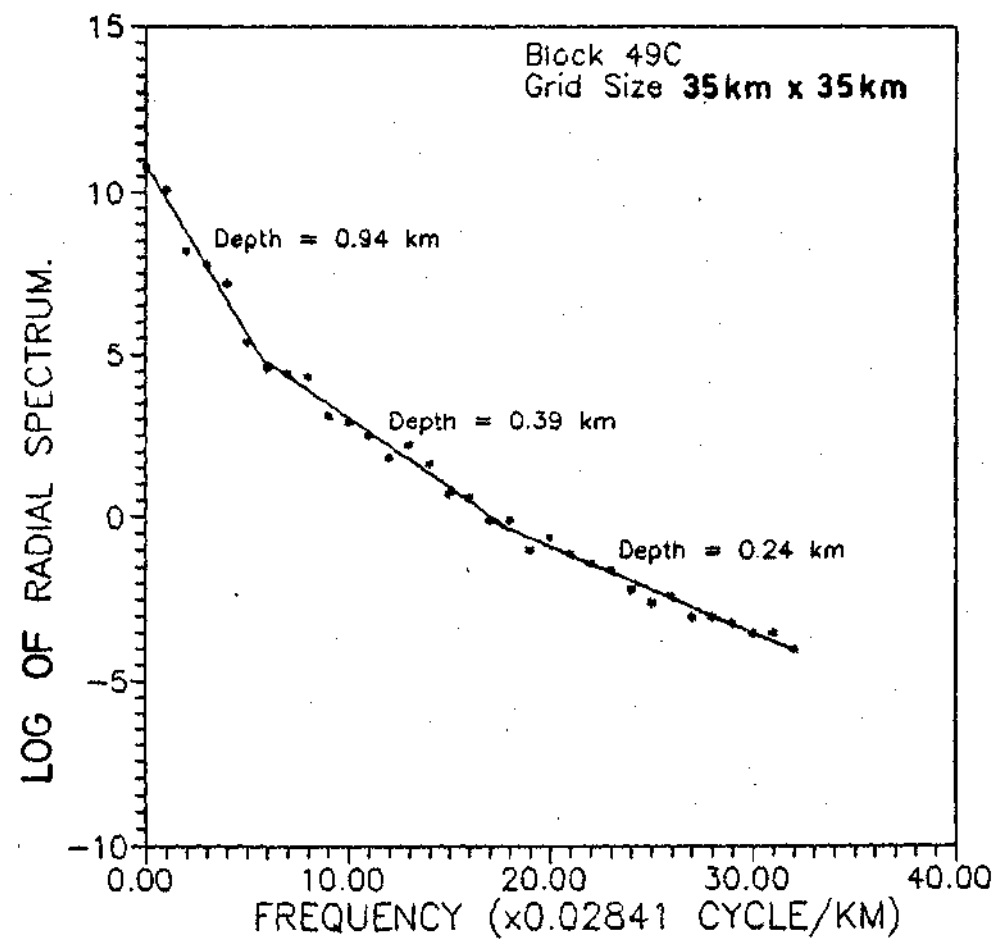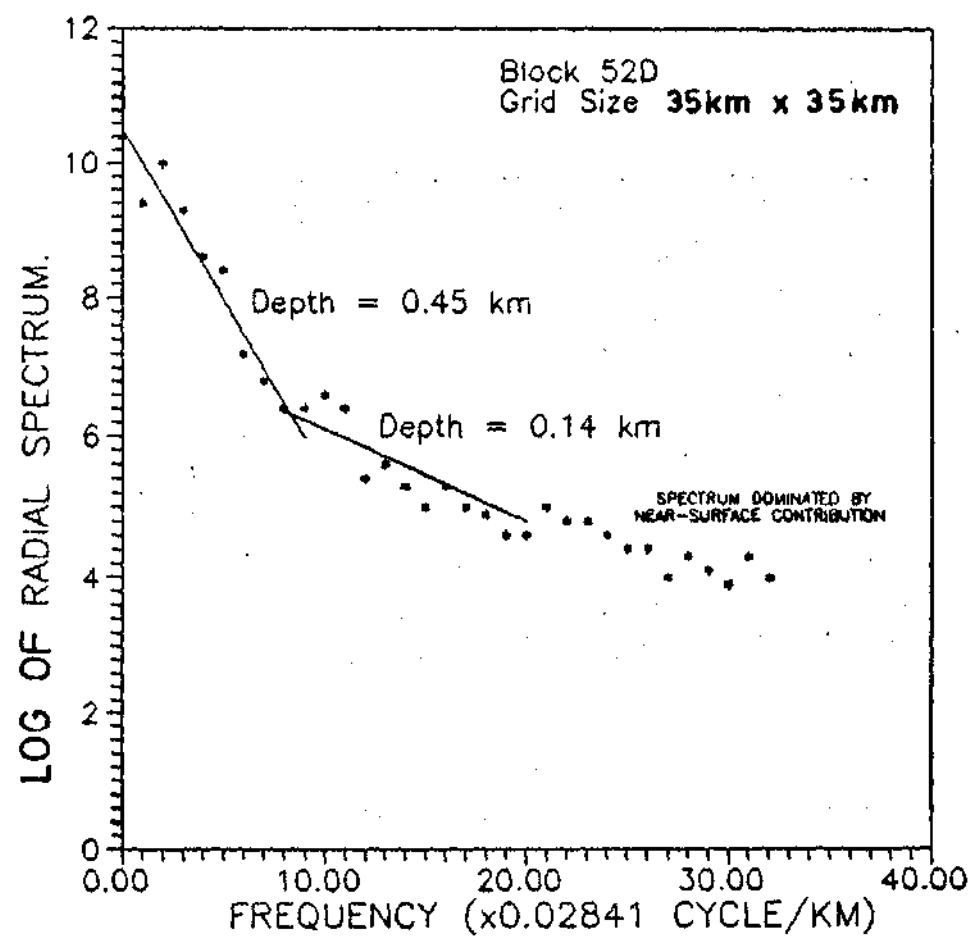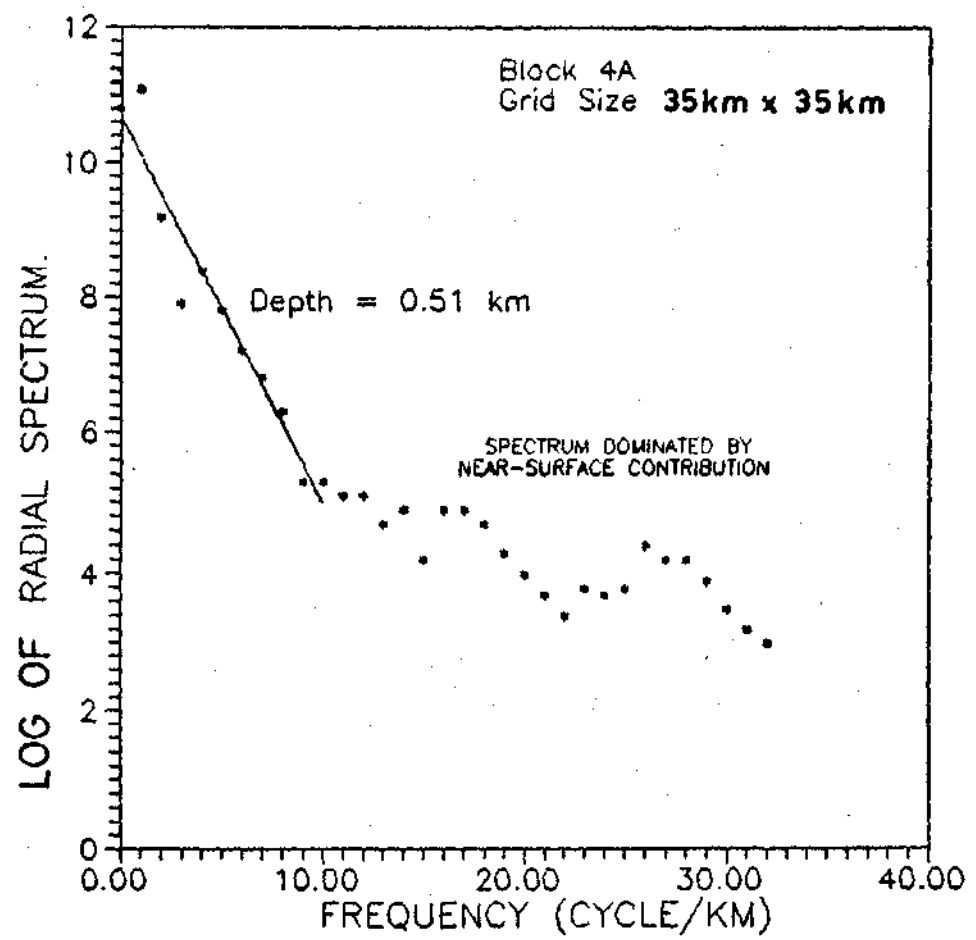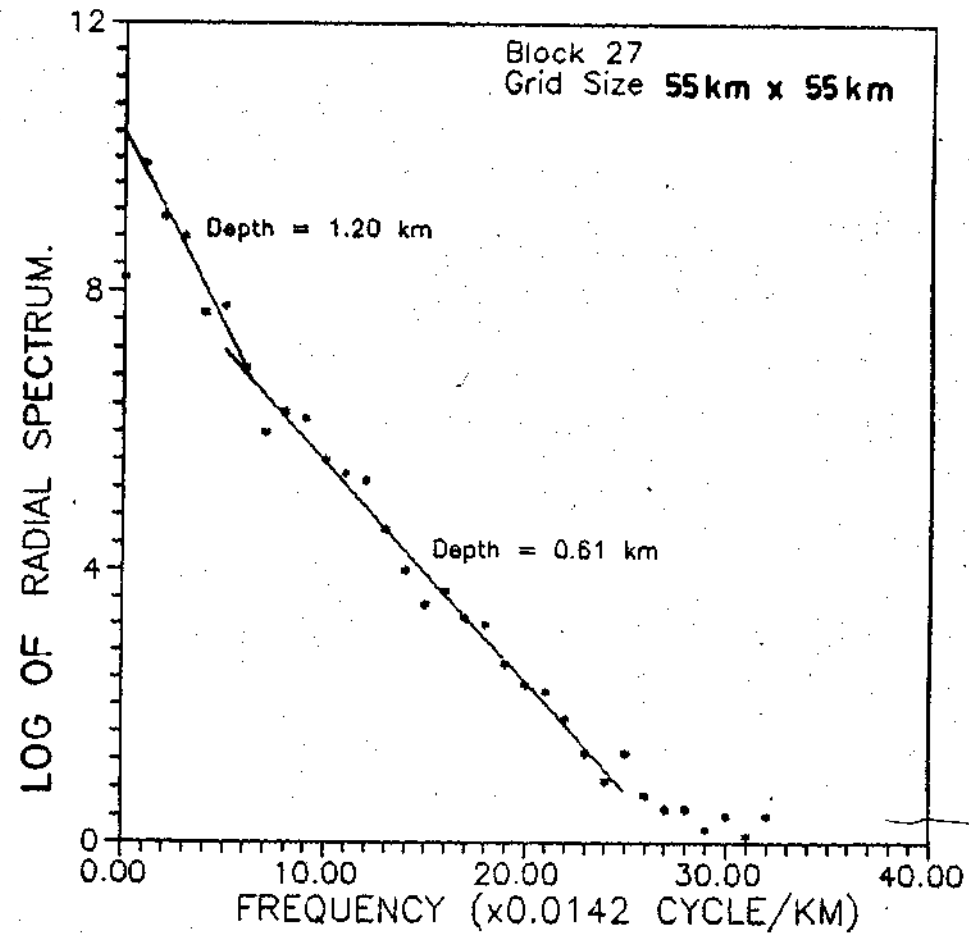
Fig. 5.13: Power Spectrum Analysis For Block 27
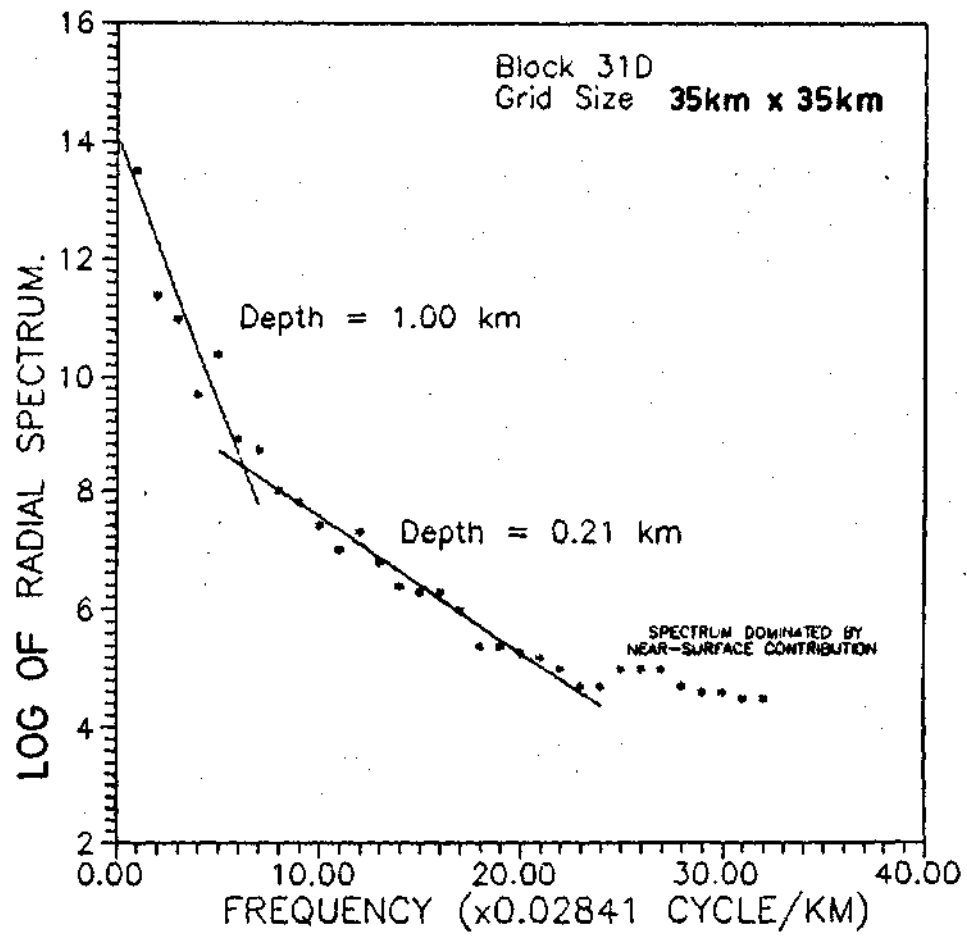
Fig. 5.14: Power Spectrum Analysis For Block 117

1	2	3	4	5
—	.2 6	.21	—	—
—	1.5 5	.6 3	.55	—
8	**9**	**10**	**11**	**12**
.2 5	.3 5	.2 6	.35	.4 1
.63	.5 8	.90	.96	.5 5
26	**27**	**28**	**29**	**30**
—	—	—	.08	—
—	.46	.29	.68	.21
—	1.05	.61	1.85	.85
31	**48**	**49**	**50**	**51**
.39	.36	.36	.30	.26
1.17	.55	.80	.83	.67
52	**71**	**72**	**73**	**94**
.17	.12	.14	.17	.18
.43	.82	.71	.87	.84
95	**96**	**116**	**117**	
.04	—	—	—	
.45	.39	.04	.35	
1.85	.70	.52	.85	

Fig.5.15: Spectral depths for 55km x 55km Blocks, corrected for flight elevation

depth estimates recorded for blocks 1, 5 and 26 because the greater part of these blocks have no data.

The spectra plots obtained using the larger map size of 55 km x 55 km show that, generally, the deep source depths for all the blocks are slightly higher than the corresponding source depths obtained for the smaller maps. For instance, the greatest depth for block 29 using the 55 km x 55 km map size (Figure 5.15) is 1.85 km and the depth values for the four 35 km x 35 km quadrants of this block (Figure 5.10) are 1.40 km, 1.25 km, 0.85 km and 0.85 km respectively. This is to be expected since the larger map (55 km) is able to resolve the deeper depths more accurately as shown by the study with synthetic data (section 4.3). A look at another block (block 30, Figure 5.15) confirms the deeper resolution of the larger map size over the smaller ones. For this block, the greatest depth was estimated to be 0.85 km using 55 square kilometre map size while the smaller map gave the mean depth of the same area as 0.51 km (Figure 5.10).

The blocks which cover the circularly shaped isolated anomaly near Dange village (latitude 5.50°, and longitude 12.80°; Figure 5.1) shows an interesting result. The spectral plots for the three selected blocks are shown in Figures 5.16, 5.17 and 5.18. The depth estimates for the low frequency segments are 1.85 km, 1.40 km and 0.85 km respectively. This implies that the magnetic sources that gave rise to this anomaly may be as deep as 1.85 km from the ground surface.
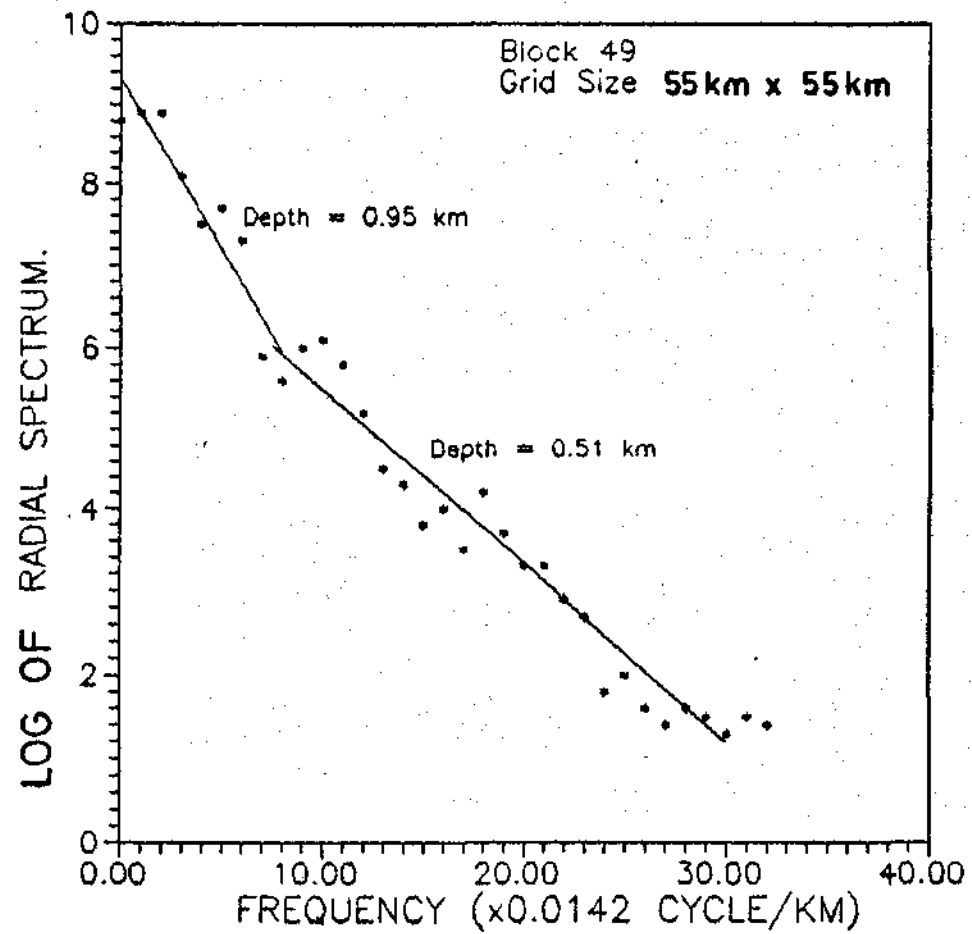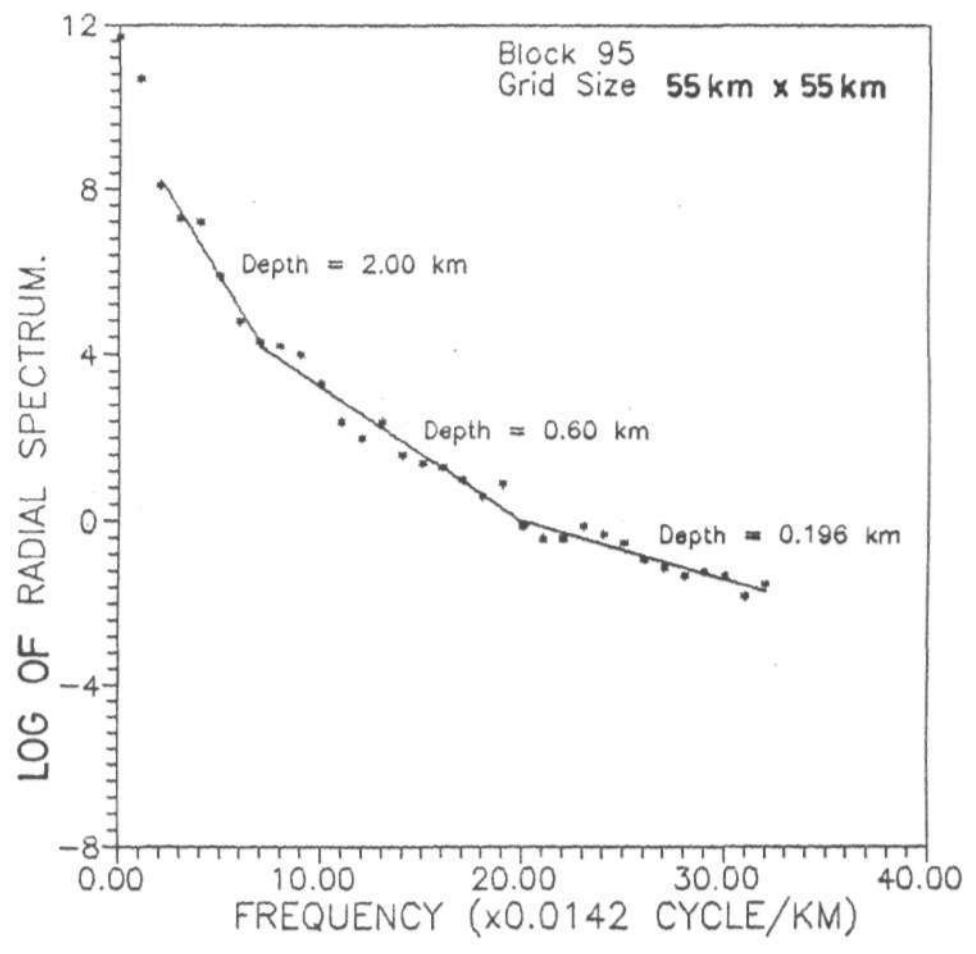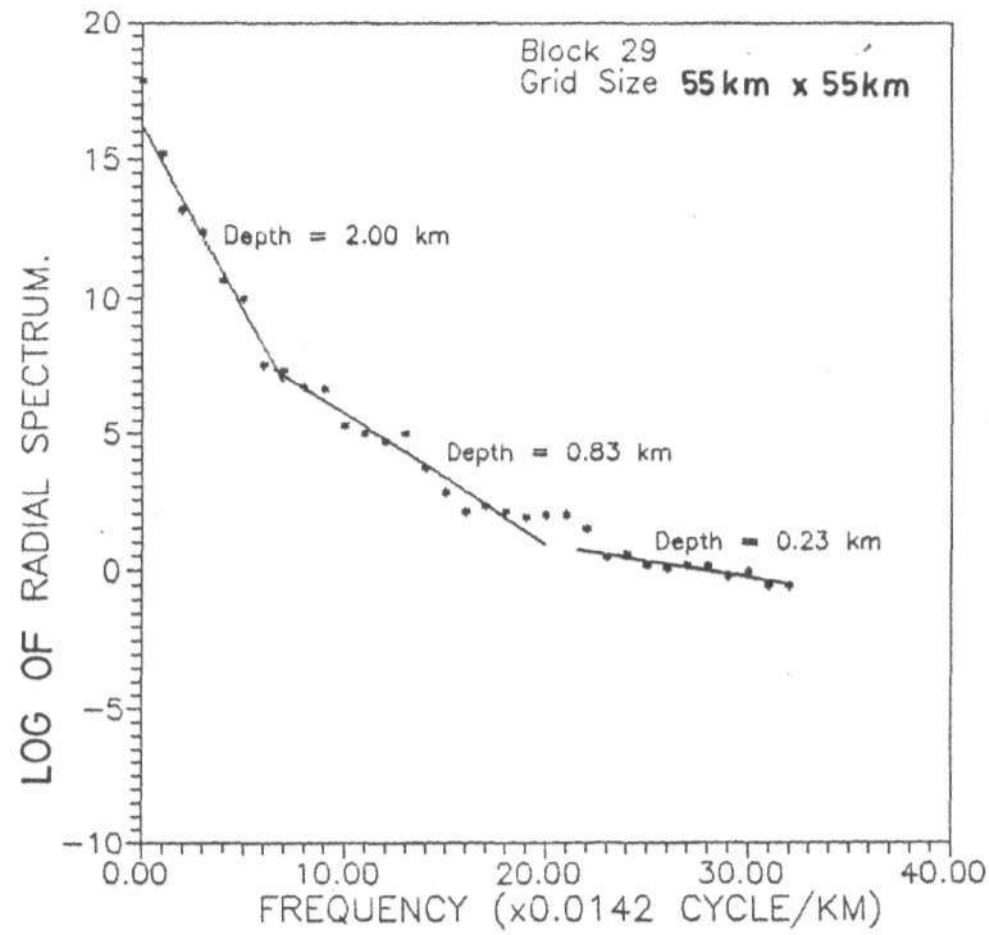
Fig. 5·16: Power Spectrum Analysis For Block 29
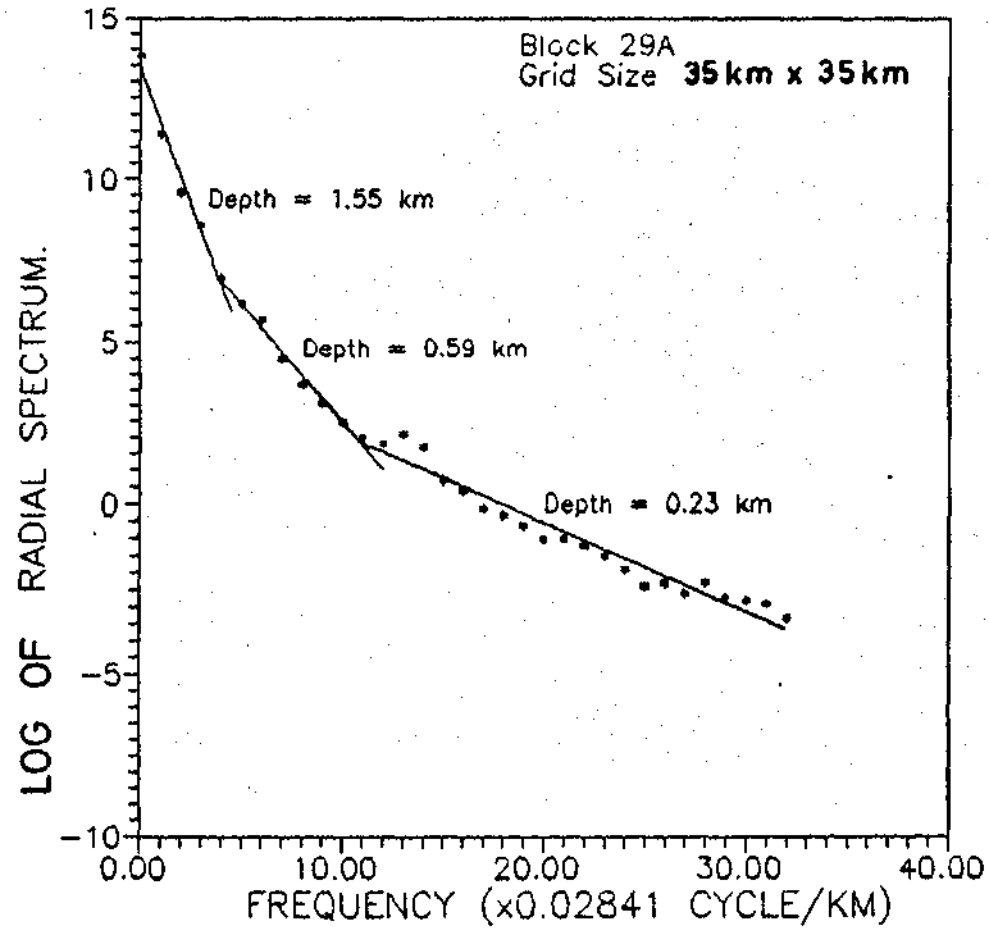
Fig. **5·17** : Power Spectrum Analysis For Block 29A
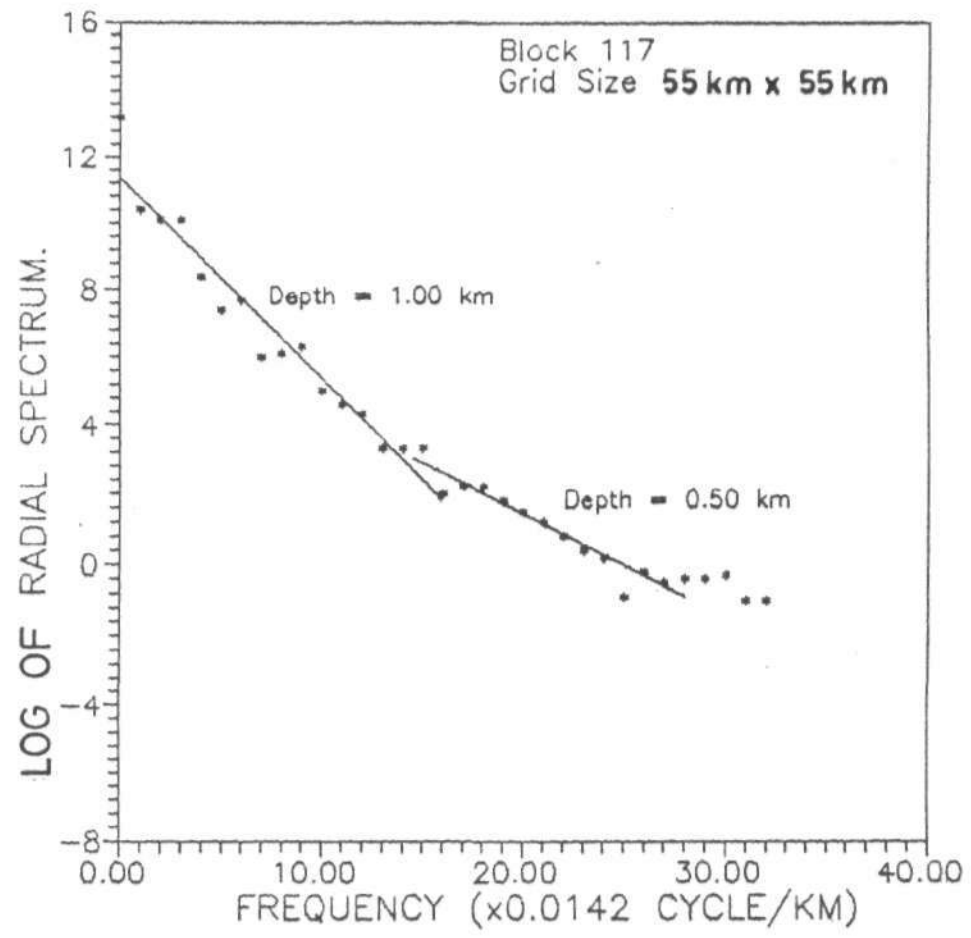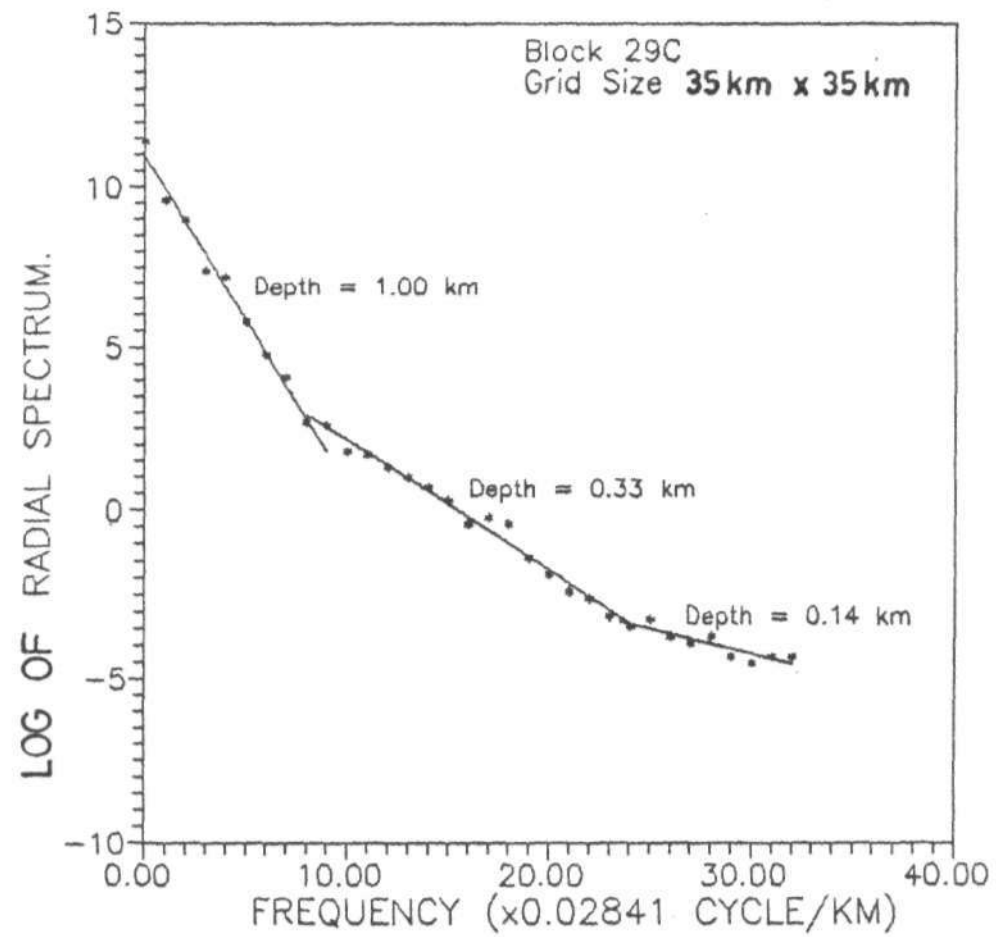
Fig. 5.18 : Power Spectrum Analysis For Block 29C

5.5.4   ANALYSIS FOR COMBINED SHEETS

The composite magnetic-anomaly map (Figures 5.1, 5.10) shows that the block sides cut through the centre or essential parts of the anomalies in respect of blocks 116 and 117, 71 and 72, 5 and 12, 2 and 9. These pairs of blocks were therefore combined and the data analysed as before. Figures 5.19 and 5.20 show the spectral plots for the first two of these combined blocks. The depth estimates for these combined blocks show that both the deeper and shallower depths are slightly higher than the value obtained for the individual separate blocks using the 55 km x 55 km map size. For example Figure 5.15 give the deeper depths for blocks 71 and 72 as 0.82 km and 0.71 km respectively and the shallower ones as 0.12 km and 0.14 km respectively. The depths for the same blocks ensuring that the anomaly is not dissected are estimated as 0.85 km and 0.20 km for the deeper and shallower sources respectively (Figure 5.19). Similarly, the analysis for the combined blocks of 116 and 117 (Figure 5.20) confirm the fact that the depths obtained from these combinations of blocks are higher than those from individual blocks (Figure 5.15).

5.6 GENERALIZED DEPTH TO BASEMENT MAP OF SOKOTO BASIN

The results of the spectral analysis of aeromagnetic data over the Sokoto basin identified two main magnetic horizons under the area. The deeper sources are represented by the
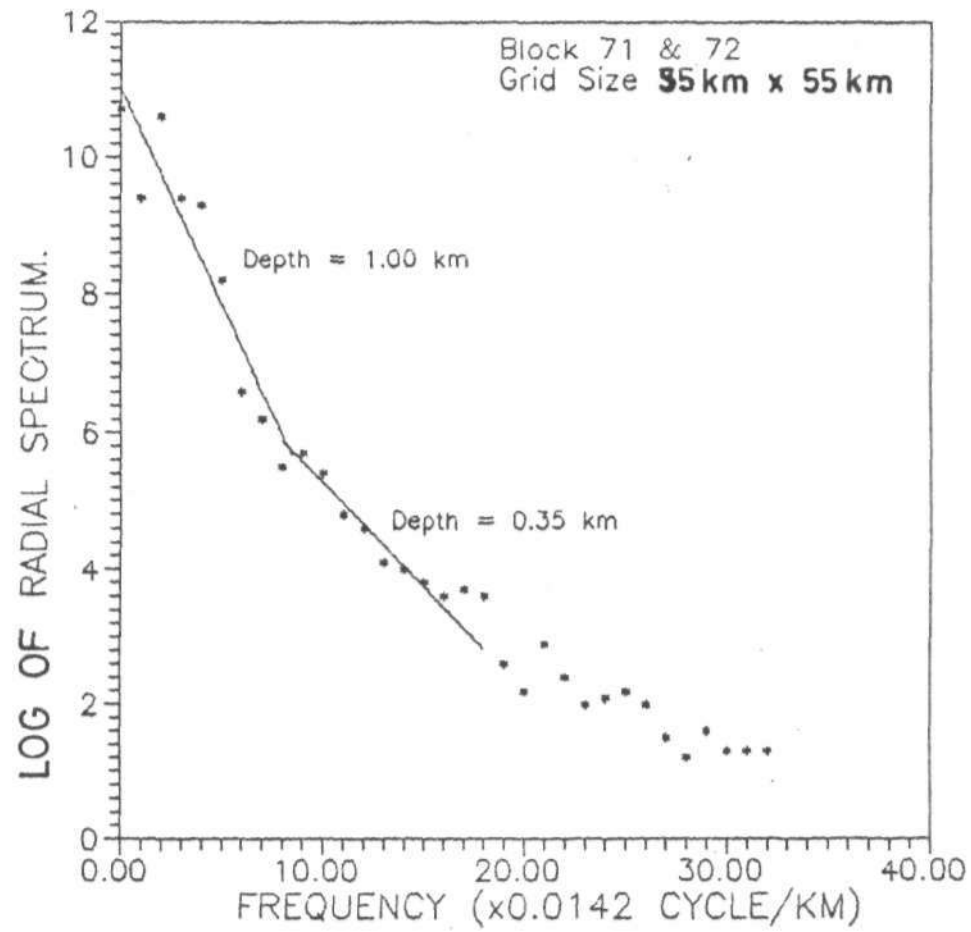
Fig. 5.19 : Power Spectrum Analysis For Block 71 And 72
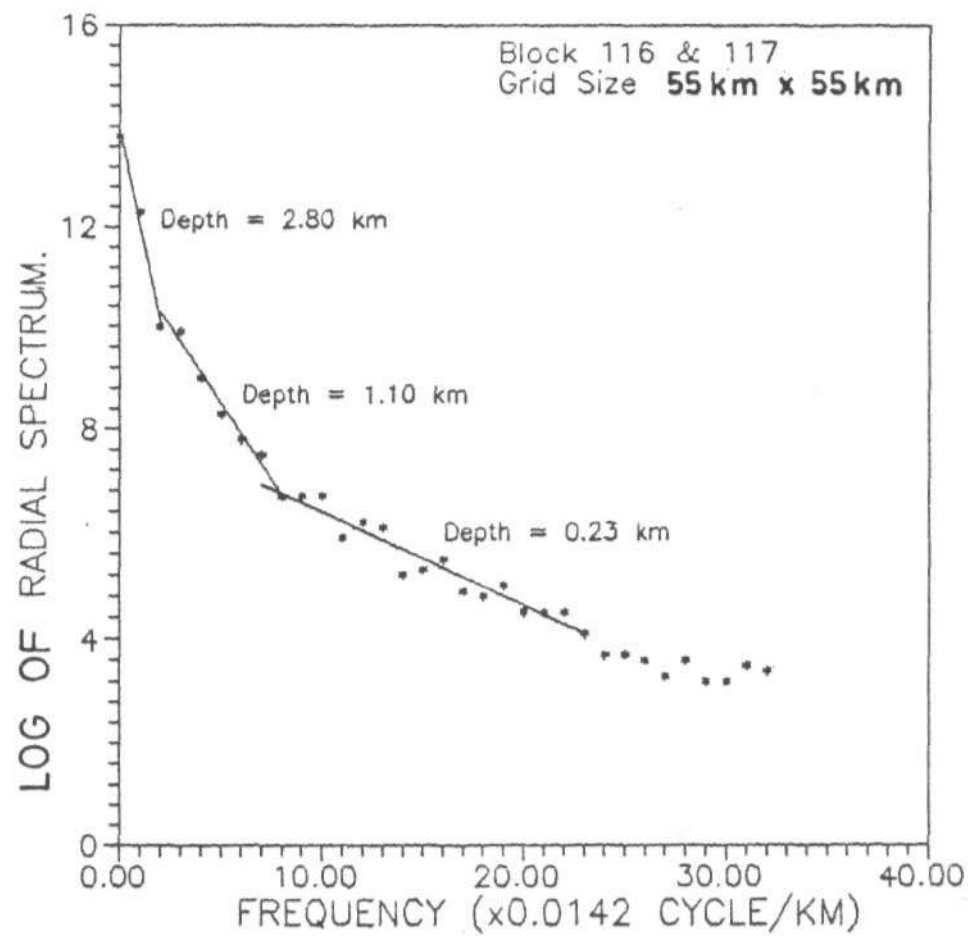
Fig. **5-20**: Power Spectrum Analysis For Block 116 And 117

low frequency segments of the spectra and shallower magnetic sources by the high frequency segment (Figures 5.10 and 5.15). The question which then arises is, which of these depth segments actually corresponds to the basement?

To resolve this problem, several factors were considered. Firstly, by reviewing all the preceding analyses, it was possible to make the following observations

a) The depths obtained using a 55 km x 55 km map size tends to give the depth limit of a particular map sheet, while each of the depths from the four quadrants refers to a section of the sheet.

b) The depths from the low frequency segment (or intermediate in some cases) appear to be of the same order of magnitude over the study area for the two map sizes, and may have resulted from the same magnetic sources. These (magnetic sources) are therefore likely to represent the basement surface.

Secondly, by comparing the above depths with depths obtained from other sources like drilling (e.g Oteze, 1979 and JICA, 1990), it was possible to fix with a little more certainty the spectral depths which correspond to basement depths. None of the boreholes drilled by JICA over the sedimentary basin reached the basement. They bottomed in well-known formations and reasonable geological estimates are available for limiting thickness of the

remaining formations. The depths of the boreholes allowed the elimination of spectral depths obtained from the shallower magnetic sources represented by the high frequency segments. Similarly, figure 5.21 is an isopach map of the sedimentary deposit in the Sokoto basin excluding the Illo Formation (Oteze, 1979). By also adding the estimated maximum thickness of Illo Formation which is 120 m (Kogbe,1979), it is possible to estimate the depth to basement at the indicated locations shown on the figure.

Table 5.1 is a summary of the extrapolated depths to basement from these two sources and the depths estimated by Umego (1990) compared with the depths obtained from the low frequency (or intermediate) segments of the energy spectra. Bearing in mind that, the maximum possible thickness of the Illo Formation which is 120 m was added to Oteze's values to obtain the above figures and that the spectral depths are average depths, the depths obtained from the low frequency segment of the energy spectra are consistent with the estimated sedimentary thickness of the basin by Oteze (1979). Similarly, examination of Table 5.1 shows that the extrapolated sedimentary depths of the basin from the JICA report of 1990 are of the same order of magnitude with the depths from the deeper magnetic sources (low frequency segment) of this study. Therefore, these depth estimates were compiled (appendix 2) together with the co-ordinates of the centre of the data blocks.
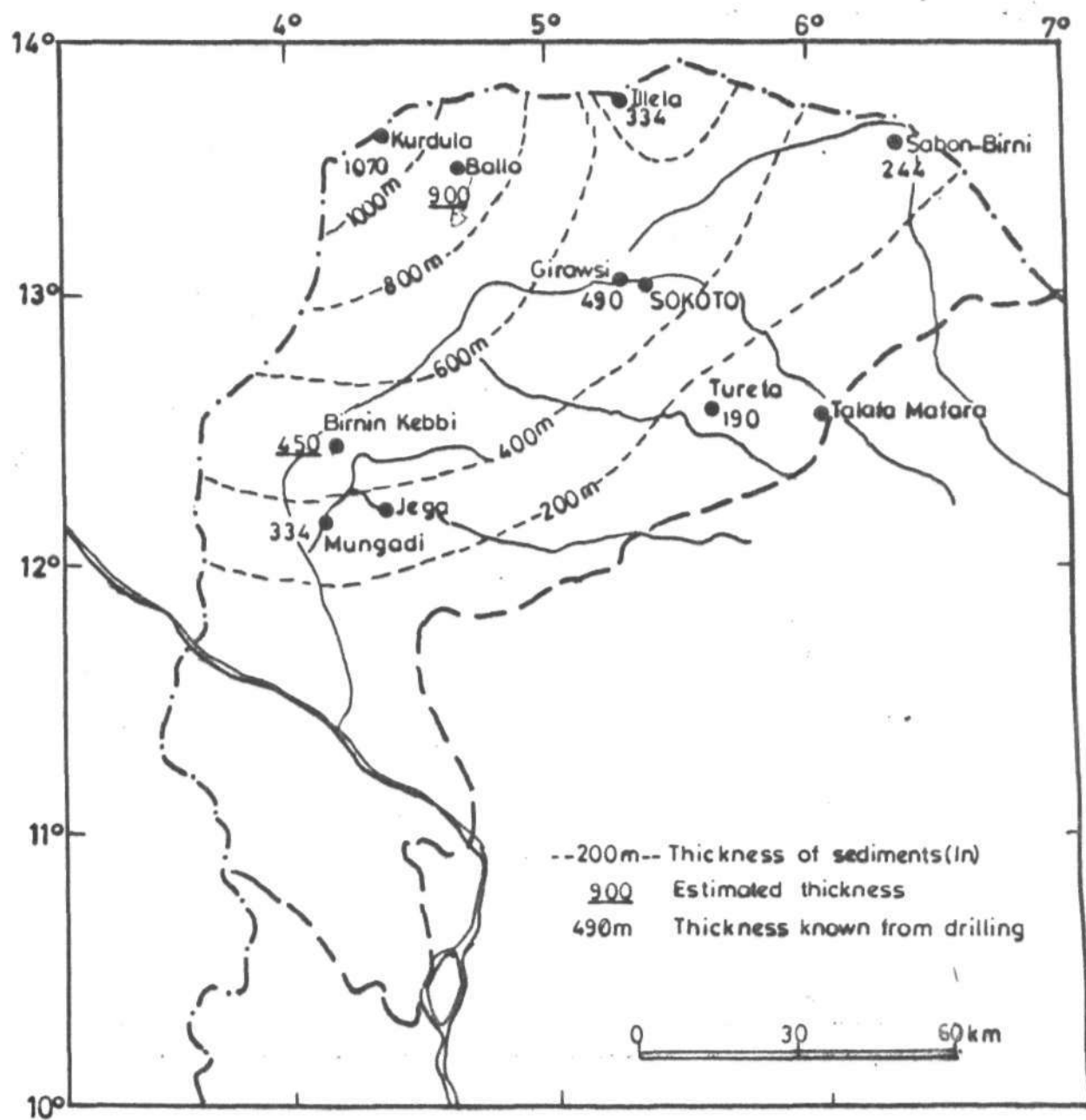
Fig·5·21: Isopachs for the sedimentary deposits in the Sokoto Basin·(Illo Formation excluded)·(After Oteze,1979)· Limiting values for depth to basement may be obtained by adding the maximum estimated value of 120m (Kogbe,1979) for the Illo formation·

Table 5.1: Correlation between the results of sedimentary thickness from the present and results extrapolated from Oteze (1979), JICA (1990) and Umego, 1990)

Sheet No	Location	Depth to Basement extrapolated from JICA (1990) (km)	Dept to Basement extrapolated from Oteze (1979) (km)	Depth to Basement estimated by Umego (1990) (km)	Depth to Basement estimated from Spectral analysis (km)
10 D	Gidan Tundu	0.347	-	1.410	0.360
27 D	Helenda	0.510	-	1.400	0.420
5 C	Kuru-Kuru	0.363	-	1.500	0.280
10 C	Sokoto	0.550	-	1.500	0.400
3 B		0.318	-	1.600	0.230
3 D	Illela	-	0.454	1.620	0.450
30 C	Tureta	-	0.310	1.410	0.290
5 D	Sabo-Birni	-	0.364	1.400	0.420
49 D	Mungadi	-	0.454	1.460	0.790

and machine-contoured to produce the generalized depth to basement map of the Sokoto Basin (Figure 5.22). The contour values represent depths to basement from the ground surface in kilometres.

5.7 DESCRIPTION AND INTERPRETATION OF THE DEPTH TO BASEMENT MAP

The depth to basement contours over the Sokoto Basin shown in Figure 5.22 suggest that the magnetic basement beneath the sediment in the basin is generally shallow and of low relief. Depths to magnetic basement range from 0.3 km to 1.4 km in the study area. The shape of these depth contours divide the study area into two zones (Figure 5.22). South of latitude 12.50°, the north-south trend is dominant while to the north of the same latitude degree the trend of the contours is diffused. The general low gradient of the depth contours even near the sediment-basement boundary suggests a gradual decrease in the basement depth from the basin towards the boundary. This is also evident on the cross-sectional views through latitudes 12.5°N and 13.0°N which are illustrated in Figures 5.23 (a) and 5.23 (b) as well as on the idealised sections of Sokoto Basin given by Kogbe (1979) and shown in Figure 24 (c).

Major basement features abstracted from Figure 5.22 are shown in Figure 5.24. A depression in the basement, immediately west of the circularly shaped anomaly near Dange village on the composite magnetic-anomaly map (Figure 5.1) is found at the
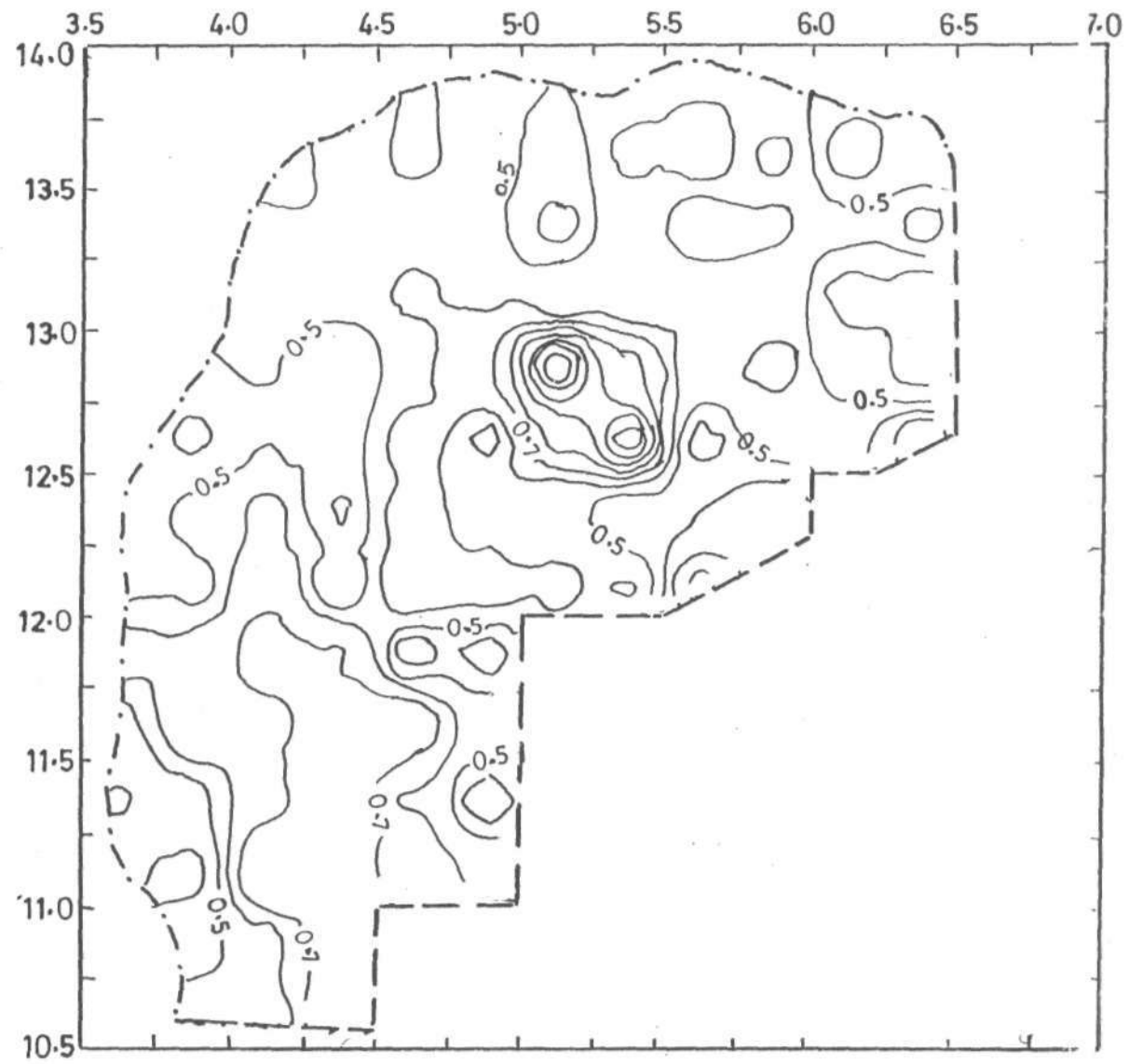
Fig.5·22: Generalised depth to basement map of Sokoto Basin
(contour interval = 0·1 km)
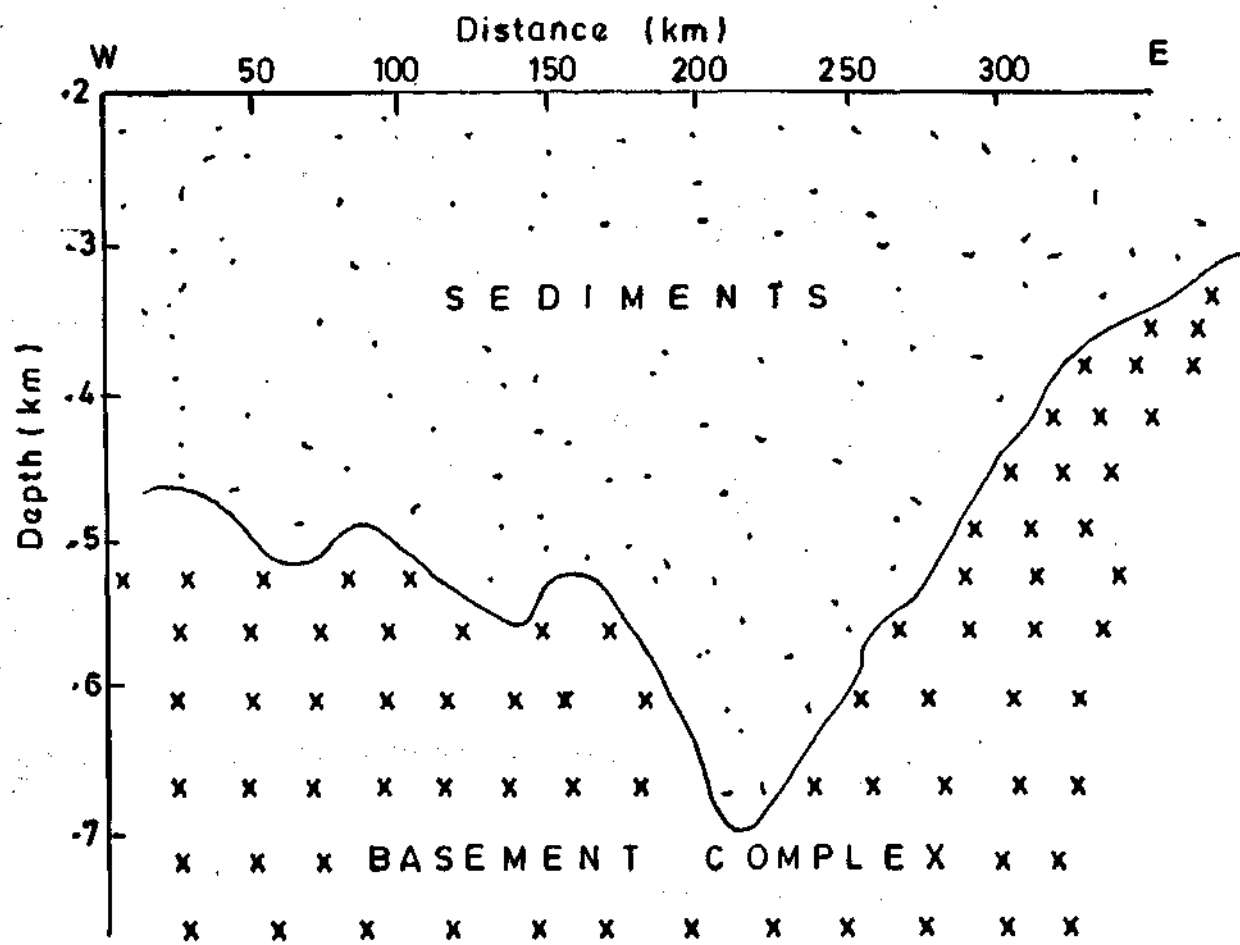
Fig.5.23(a): Sectional view of the basement surface through
latitude 12.5°N
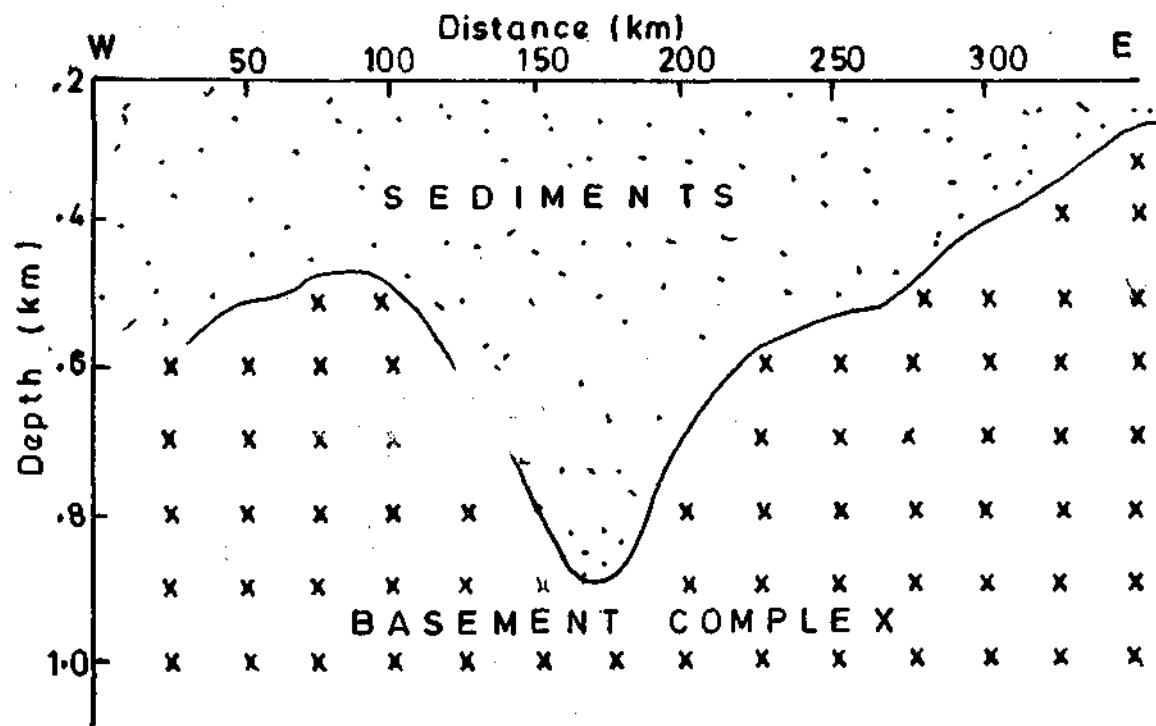
Fig.5.23(b): Sectional view of the basement surface through
latitude 13.0°N
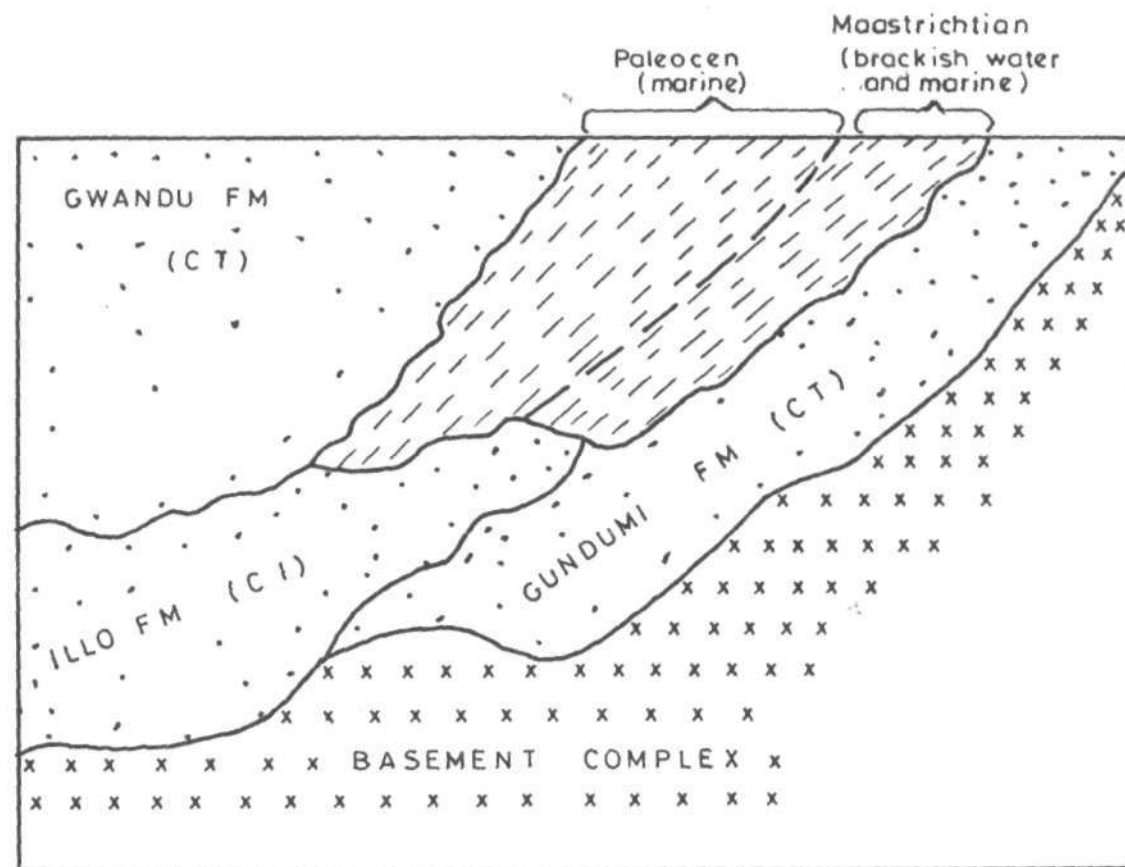
Fig.5·2₃(c): Idealised section of the Sokoto Basin (After Kogbe, 1979)
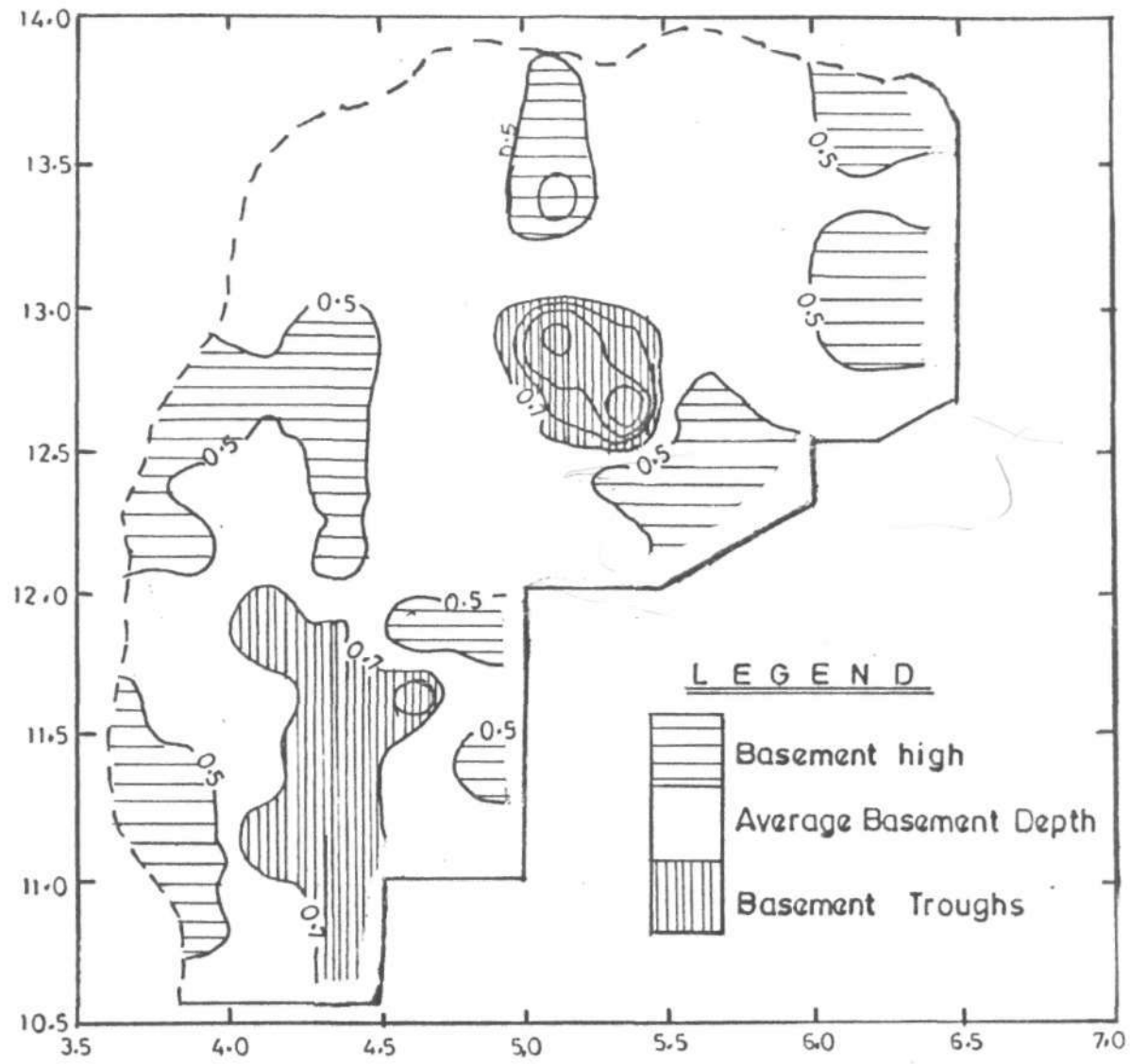
Fig. 5·24: Major features of the basin abstracted from Fig. 5·22

centre of the map of major features of the basement (Figure 5.24). The depression varies in depth between 0.6 km and 1.4 km. A depth section along latitude 12.75° which is shown in Figure 5.25 shows the bowl shape form for this Dange depression. The spectrally estimated depth of 1.4 km for this features agrees favourably well with the gravity result of Umego (1990) which estimated the depression to have a depth of 1.0 km. Another basement feature revealed by the map is in the form of a N-S trending troughs and ridges located in the south-western part of the study area. The undulating shape of this feature suggests gentle folding of the sub-surface basement rocks. The two sectional views through latitudes 12.5°N and 13.0°N which are illustrated in the Figures 5.23 (a) and 5.23 (b) help to confirm this suggestion. It may therefore be concluded that the basement rocks underlying the basin have been gently deformed into anticlines and synclines. Since the synclines and other depressions are filled with more than average thickness of the sediments, they may therefore be probable targets for groundwater exploration.

A comparison of the map of the major features of the basement with the composite magnetic-anomaly map shows that the short wavelength area in Figure 5.1, especially, in the north-west, north-east and south-west are found to correspond closely to the shallow depth features (basement high) at the same locations in Figure 5.25. Similarly, the long wavelength anomaly in the southern part of the composite magnetic anomaly -
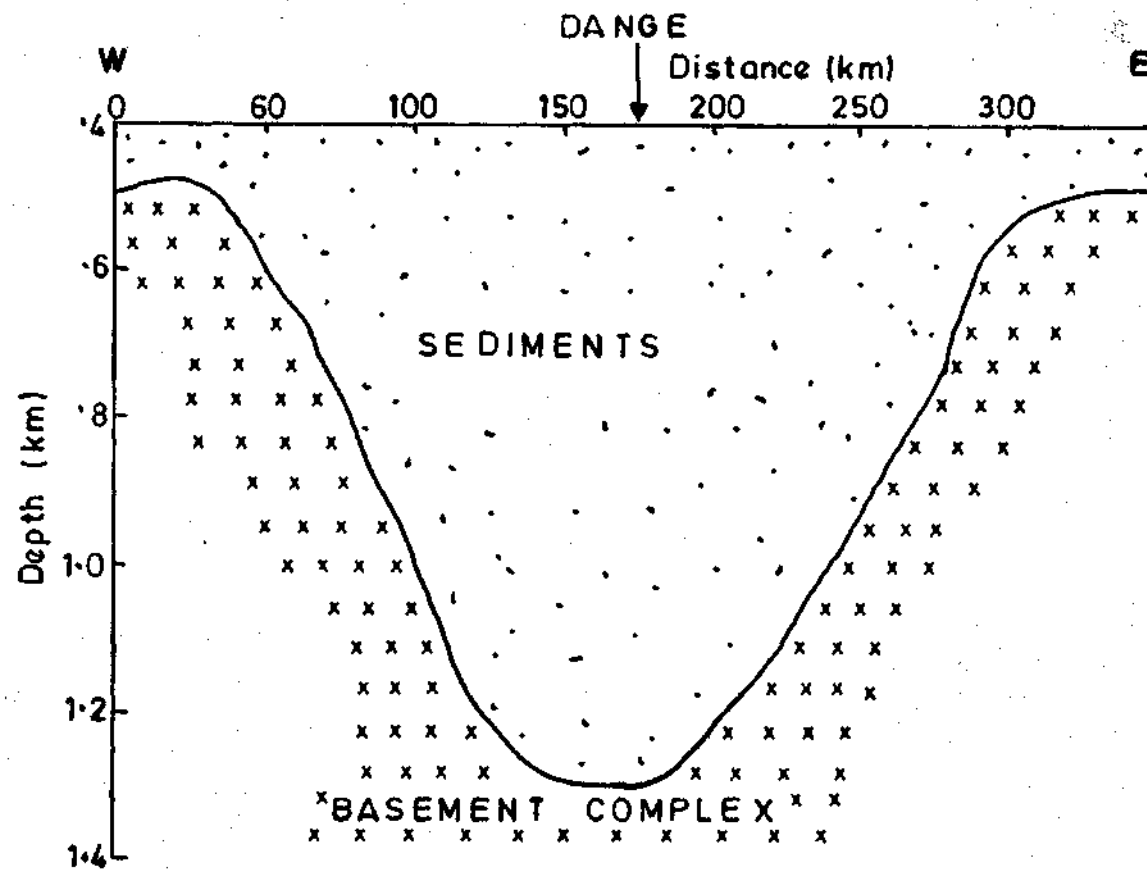
Fig.5.25 : W-E. sectional view of the basement surface through latitude 12.75° N

map coincide with the N-S trending troughs in the same area in Figure 5.24, while the central part of Figure 5.1 is smooth contours with low gradients correspond to the location of the circularly shaped basement depression on the map of the basement features. Since the short wavelength anomalies usually indicate shallow magnetic sources and the reverse is true for the long wavelength anomalies there is a very good correlation between the two maps (Figures 5.1 and 5.24).

5.8 TECTONICS AND ORIGIN OF THE SOKOTO BASIN

Kogbe (1981) observed that the Iullemmenden Basin in its totality is a cratonic basin created by tectonic epierogenic movements and commenced around the beginning of the Palaeozoic and continued until the upper Cretaceous, when the opening of the Goa Trench was achieved. However, a set of NE-SW and NW-SE conjugate strike-slip fracture systems interpreted to be of tectonic origin was identified in Sokoto Basin by Ananaba (1983) and Oluyide (1988).

The N-S trending troughs and ridges shown in the south-western part of the study area (Figure 5.24) show that, the stresses which acted on this region has a major east-west component. This, coupled with the diffused nature of the depth contours are indications that the basement has been subjected to at least two tectonic events in the past. Also there is the possibility of a gentle folding of the sub-surface basement

rocks as revealed by the two cross-sectional views through latitudes 12.5°N and 13.0°N (Figure 5.23 (a) and (b)). These two events (tectonic event, which usually occur before sedimentation, and folding of the underlying rocks) are indications of movements of the underlying structures of the basin. Thus if the movement of the underlying rocks of the basin took place as inferred, then the south-eastern sector of the Iullemmenden Basin, locally known as the Sokoto basin in Nigeria probably originated from the tectonic movement within the Precambrian Basement rocks.

CHAPTER SIX

SUMMARY AND CONCLUSION

6.1 INTRODUCTION

The sedimentary basin of North-Eastern Nigeria consists predominantly of a gentle undulating plain with an average elevation varying from 250 to 400 metres above sea level (Kogbe, 1979). This basin is part of the much larger, nearly circular Mesozoic basin known as Iullemmeden basin of West-Africa (Figure 2.1). Structural information on the sub-surface basement made available from the work of Ogile and Anderson (1965), Oteze (1979), Kogbe (1979, 1981) and JICA (1990) is scanty and highly generalised. Most previous geophysical surveys of the basin were targeted at the various aquifers within the sedimentary strata with the result that very little is known about the structures of the underlying basement rocks. The only comprehensive geophysical investigation of the structures of the basin using gravity and magnetic methods was by Umego (1990). However, he noted a significant difference in the depth to basement estimates from both methods, the magnetic depth estimates being generally larger (in the two cases). At one location for instance, comparison showed estimates of 0.8 km and 1.6 km for the gravity and magnetic methods respectively. The present work was therefore aimed at resolving these differences as well as

contributing to the general knowledge of the regional sub-
surface structures of the basin by mapping the basement
topography and identifying other major sub-basement structures.

6.2 DISCUSSIONS AND CONCLUSIONS

Two dimensional spectral analysis of magnetic
interpretations was applied to determine depth to magnetic
basement in the Sokoto basin. There exists three distinct
identifiable sources of error in this approach. One relates to
the fact that the errors in the source depth determination here
increases with the depth of the source and are related to the
map size. A map size of about 12.5 times the target depth
contains wavelengths of up to $T/2$ (T = crustal thickness).
Naidu (1970) therefore considers the minimum map size to be at
least 40 - 50 times the target depth. This was taken care of
during the course of this work by increasing the map size from
35 km x 35 km to 55 km x 55 km size when considering the deeper
magnetic sources. Digitization spacing also affect the
retrieval of true spectrum and therefore the interpretational
fidelity. The sampling interval used during the collection of
data used for this work is 550 m. This spacing of 550 m
directly imposes a Nyquist frequency of 1/1.1 km . The spacing
was found adequate since we are concerned with the source
originating from not more than 2 km in thickness (Umego, 1990).
The third problem relate to the identification of different

linear segments in the power spectrum. This was overcome by (a) considering the boreholes results, and (b) carefully studying the distribution of anomalies over the study area and the spectral plots that are related to them before choosing the middle segments (or second segments in most cases) as the segments corresponding to the basement depth. Moreover, Pal, *et al*. (1978) suggested that one possible way to overcome this problem would be to select the middle portions of the power spectrum for depth interpretations as the high frequency components indicate the regional effect.

The results of the spectral analysis of aeromagnetic data over the basin suggest the existence of two main source depths in the depth range considered under the area. The deeper source depth lie at a depth that varies between 0.3 km near the boundary with the basement complex and 1.85 km at the centre of the basin. These deeper sources represented by the low frequency components of the spectrum are considered to reflect the depth to the magnetic basement. The shallow magnetic horizon represented by the high frequency components indicate either the near surface contributions or the noise effect.

A generalized depth to magnetic basement map (Figure 5.22) was produced from the depth results of the spectral analysis over the study area. The map reveals a generally shallow basement surface deepest at the centre of the study area and decreases gradually towards the eastern and western boundaries. Also the depth to basement map reveals that the basement rocks

in this region must have undergone at least two tectonic events which has resulted in the N-S structural features and the diffused nature of the depth contours shown on this map. The depth estimates (obtained in this study) are accurate to within 10% and this sets an upper limit of 1.85 km as the maximum depth to the magnetic basement in Sokoto basin. One important significance of this result is in the consideration of the hydrocarbon accumulation potential of the basin. According to Kogbe (1979), the probable source beds in the basin are the Marine Maastrichtian Rima and Sokoto groups which overlie the continental beds at an estimated maximum depth of 900 m. Wright, *et al*. (1985) had shown that if all other conditions for hydrocarbon accumulation are favourable, and the average temperature gradient of $1^\circ C$ per 30 m which obtain in Niger Delta is applicable, then the minimum thickness of sediment to achieve the threshhold temperature of $115^\circ C$ for the commencement of oil formation from organic remains would be 2.3 km. Based on the shallow depth of the probable source beds in the basin, the prospect for the hydrocarbon accumulation is therefore not promising.

A comparison of the basement depth estimates of this work with the results obtained by Umego (1990) using Werner Deconvolution method shows that Umego's analysis gave basement depth of between 1.2 km and 1.8 km while the present study estimated the basement depth to be between 0.3 km and 1.4 km. Possible causes of the discrepancy in the depth estimates by the

two methods might be any of the followings:

1) Werner deconvolution method fails for profile segments where anomalies significantly overlap (Birch, 1985).

2) Birch (1985) also showed that Werner deconvolution method will not give a good result where noise contaminates the measurements and that noise seems less detrimental to good result in spectral method.

On the basis of comparisons with the borehole and geological extrapolated depths, it can be concluded that the depths obtained using the spectral method are reasonably reliable. It may also be concluded that the Werner technique is not very suitable for depth to basement determination because the variation in the basement topography cannot accurately be approximated by dykes or the geologic contact which are the basis of the Werner technique.

6.3 RECOMMENDATION

1) Problems relating to the origin and structures of the Sokoto basin cannot be adequately addressed without considering the larger Iullemmeden basin of which Sokoto Basin forms a part. It would, therefore, be desirable to carry out a more detailed study of the entire Iullemmeden basin with

techniques based on spectral analysis of magnetic data. The objective of this would be to produce a depth to basement map of the entire basin with a view to studying the underlying structures and thus infer the origin of the entire basin.

2) Adequate control to geophysical results from a few boreholes which reach the basement are highly needed in the study area. It is therefore recommended that the Federal Government through its agencies should respond positively in this regard by sinking a few boreholes which reach the basement of the basin.

REFERENCES

Ananaba, S.E. (1983). Evaluation of remote sensing application to geophysical studies in Nigeria. Unpublished Ph.D Thesis. Ahmadu Bello University Zaria, Kaduna.

Ananaba, S.E. and Ajakaiye, D.E. (1987). Evidence of tectonic control of mineralization in Nigeria from lineament density analysis: A Landsat Study. **Int. J. Remote Sensing** 8, 10: 1445 - 1453.

Ball, E. (1980). An example of very consistent Brittle deformation over a wide intercontinental area. The late Pan-African fracture system of Tuareg and Nigerian Shield. **Tectonophysics** 61: 363 - 379.

Bath, M. (1947). **Spectral Analysis in Geophysics**, Elsevier Pub. Co. Amsterdam, 563pp.

Bhattacharyya, B. K. (1965). Magnetic anomalies due to prism-shaped bodies with arbitrary polarization, **Geophysics** 29: 517 - 531.

Bhattacharyya, B. K. (1966). Continuous spectrum of the magmatic field anomaly due to a rectangular prismatic body, **Geophysics** 31: 97 - 121

Birch, S.F. (1985): Bedrock Depth Estimates from Ground Magnetometer profiles: **Groundwater** 22(4): 427 - 432.

Dobrin, M.B. (1976). **Introduction to Geophysical prospecting**. McGraw-Hill. New York, 630 pp.

Grant, F.S. (1978). Review of data processing and interpretation method in Gravity and Magnetics 1964-1971. **Geophysics**, 37(4): 647-661.

Hahn, A; Kind, E.G. and Mishra, D.C. (1976). Depth estimation of Magnetic sources by means of Fourier amplitude spectra. **Geophysical Prosp**. 24: 278 - 308

Jain, S. (1976). An automatic method of direct interpretation of magnetic profiles. **Geophysics** 41(3): 531-541.

Japanese International Cooperation Agency (JICA) (1990). The study of groundwater development in Sokoto State of Nigeria: Progress Reports Vol. 3, 4 and 5.

Jones, B. (1984). The sedimentary rocks of Sokoto province. **Bull. Geol. Survey of Nigeria** No.18: 1-72.

Kogbe, A.C. (1979). Geology of the South-eastern (Sokoto) sector of the Iullemmeden Basin. Bulletin, Department of Geology. Ahmadu Bello University, Zaria, Nigeria. 420pp.

Kogbe, A.C. (1981). Cretaceous and Tertiary of the Iullemmeden Basin in Nigeria (West Africa). **Cretaceous Research**. 2: 129-186.

Krumbein, W.C. (1959). Trend surface analysis of contour - type maps with irregular control-point spacing. **Journal of Geophys. Research**. 64(7): 823-835.

McCurry, P. (1976). The Geology of the Precambrian to lower Palaeozoic rocks of north-western Nigeria - a review. In: Kogbe, C.A. (Ed.) **Geology of Nigeria** - Elizabethan Pub. Co., Lagos 15 - 39.

Misha, D.C. and Naidu, P.S. (1974). Two-dimensional power spectral analysis of aeromagnetic fields. **Geophys. Prosp.**, 22: 345-353.

Naidu, P.S. (1970a). Statistical structure of aeromagnetic field. **Geophysics** 35 (2): 279 - 292.

Naidu, P.S. (1970b). Fourier transform of large scale aeromagnetic field using a modified version of fast Fourier transform. **Pageoph.**, 81(4): 17-25.

Negi, J.G; Agrawal, P.K. and Rao, K.N.N. (1983). Three-dimensional model of the Koyan area of Maharshaitra state (India) based on the spectral analysis of aeromagnetic data. **Geophysics.** 48 (7): 964-974.

Odeyemi, I. B. (1988). Lithostratigraphy and structural relationships of the Upper Precambrian metasediments in Igarra area, south-western Nigeria. In: (Oluyide, P.O., ed.) **Geology of Nigeria**, Geological Survey of Nigeria, Kaduna 111 - 125.

Ojo, S.B. (1986). Two DFFT. a two-dimensional spectral Depth program. Department of Physics, Ahmadu Bello University, Zaria, Nigeria.

Oluyide, P.O. (1988). Structural trends in the Nigerian Basement Complex. In Oluyide P.O (Ed.) **Precambrian geology of Nigeria** - Geological Survey of Nigeria Kaduna.

Osazuwa, I.B. (1985). The Establishment of a Primary Gravity Network for Nigeria, Ph.D. Thesis, Ahmadu Bello University, Zaria Nigeria, 320 pp.

Osazuwa, I.B. (1992). The Nigerian Standard Gravimeter Calibration line. **Survey Review.** 31 (245). 397-408.

Oteze, G.E (1979). The hydrology of the North western Nigerian basin. In: Kogbe, C.A. (Ed.) **Geology of Nigeria** Elizbethan Pub. Co. Lagos 373-390.

Oyawoye, M.O. (1964). The geology of the Nigerian basement complex. **J. Mining Geol. and Metalls. Soc.** 1: 87-102.

Pal. P.C; Khurana, K.K. and Unikdrishman, P. (1978). Two examples of spectral approach to source depth estimation in gravity and magnetics **Pageoph.**, 117: 772 - 783.

Raeburn, C. and Tattam, C. M. (1930). A preliminary note on sedimentary rocks of Sokoto Province. **Bull Geol. Survey of Nigeria** 13: 57 - 60.

Rao, D.B. and N. Ramesh Babu (1991). A rapid method for three-dimensional modelling of magnetic anomalies **Geophysics** 56, 11: 1729-1737.

Spector, A and Grant, F.S. (1970). Statistical models for interpreting aeromagnetic data. **Geophysics** 35: 293-302.

Telford, W.M.N., Geldart, L.P., Sheriff, R.E. and Keys, D.A. (1976). Applied **Geophysics.** Cambridge University Press Cambridge, 860pp.

Umego M.N. (1990). Structural interpretation of Gravity and aeromagnetic anomalies over Sokoto Basin. Northwestern Nigeria. Unpublished Ph.D Thesis Ahmadu Bello University, Zaria, Nigeria.

Uwa, E. J. (1984). Investigation of radiometric anomalies by nuclear and other methods: A case study of Sokoto Basin of Nigeria. Unpublished Ph.D Thesis, Ahmadu Bello University, Zaria, Nigeria.

Vacquier, V., Steenland, N. C. Henderson, R. G. and Zietz, I. (1951). Interpretation of aeromagnetic maps. Geol. soc. am., Mem., 47: 151pp.

Verheijen, P.J.T. and Ajakaiye, D.E. (1978). A gravimeter calibration line for Nigeria **Survey Review** 24 (190): 373 - 380.

Wrigh, J. B. (1968). South Atlantic Continental drift and the Benue Trough. **Tectonophysics** 6 (4): 301 - 310

Wright, J. B., Hastings, D. A., Jones, W. B. and Williams, H. R. (1985). **Geology and Mineral Resources of West Africa**, George Allen and Urwin, London 90 - 120.

THE COMPUTER PROGRAMME USED TO GENERATE ATHE MAGNETIC FIELD DUE
TO THE EIGHT PRISMATIC BODIES

```
PROGRAM TREDMOD
C
C        THIS PROGRAM COMPUTES THE MAGNETIC ANOMALIES FOR A PRISM
C        A B H ARE THE COORDINATES OF A VERTICAL PRISM
C        H1,H2 - DEPTH TO TOP AND BOTTOM OF PRISM RESP,
         EI-INTENSITY OF
C        MAGNETIZATION OF PRISM; P,Q,R - DIRECTION COSINES OF FIELD
C        AI,D - INCLINATION AND DECLINATION OF GEOMAGNETIC FIELD
C        AIO,DO - INCL. AND DECL. OF MAGNETIZATION VECTOR OF PRISM
C        XORIG,YORIG - COORDINATES OF FIRST POINT
C        LX,LY,DELTAX,DELTAY - NO OF GRID POINTS AND SPACINGS
C        ALONG X & Y AXIS RESP., XAXIS POINTS TOWARDS GEOGRAPHIC
         NORTH
C        THETA - ANGLE BY WHICH SIDE OF PRISM DEVIATES FROM
         GEOGRAPHIC NORTH
C        CGSK  - MAGNETIC SUSCEPTIBILITY OF PRISM IN CGS UNITS
C        TF    - INTENSITY OF GEOMAGNETIC FIELD IN nT
C
C
         DIMENSION DELTAT(64,64)
         PI-3.14159265
         FACT=PI/180.0
         READ(5,30)AI,D,TF,XORIG,YORIG,DELTAX,DELTAY,LX,LY,NBODY
         WRITE(6,1000)
         WRITE(6,1001)AI,D,TF,XORIG,YORIG,DELTAX,DELTAY,LX,LY,NBODY
         DO 5 IX-1,LX
         DO 5 IY-1,LY
         DELTAT(IY,IX)-0.0
    5    CONTINUE
         AI-AI*FACT
         D-D*FACT
C
         DO 200 IB-1,NBODY
WRITE(6,1002)
         READ(5,40)A1,A2,B1,B2,H1,H2,CGSK,AIO,DO,THETA
         EI-CGSK*TF/100.0
WRITE(6,1003)IB,A1,A2,B1,B2,H1,H2,CGSK,AIO,DO,THETA,EI
         AIO-AIO*FACT
         DO-DO*FACT
         THETA-THETA*FACT
         P=COS(AI)*COS(D-THETA)
         Q-COS(AI)*SIN(D-THETA)
         R=SIN(AI)
         S-COS(AIO)*COS(DO-THETA)
         T-COS(AIO)*SIN(DO-THETA)
         U-SIN(AIO)
         G1-EI*(T*R+U*Q)
         G2-EI*(S*R+U*P)
```

```
      G3=EI*(S*Q+T*P)
      G4=EI*(U*R-T*Q)
      G5=EI*(U*R-S*P)
      DO 100 IY=1,LY
      YSTAT=FLOAT(IY-1)*DELTAY+YORIG
      DO 100 IX=1,LX
      XSTAT=FLOAT(IX-1)*DELTAX+XORIG
      YPRIME=-XSTAT*SIN(THETA)+YSTAT*COS(THETA)
      XPRIME=XSTAT*COS(THETA)+YSTAT*SIN(THETA)
      ALPHA1=A1-XPRIME
      ALPHA2=A2-XPRIME
      BETA1=B1-YPRIME
      BETA2=B2-YPRIME
      R1=SQRT(ALPHA1**2+BETA1**2+H1**2)
      R2=SQRT(ALPHA1**2+BETA1**2+H2**2)
      R3=SQRT(ALPHA2**2+BETA1**2+H1**2)
      R4=SQRT(ALPHA2**2+BETA1**2+H2**2)
      R5=SQRT(ALPHA1**2+BETA2**2+H1**2)
      R6=SQRT(ALPHA1**2+BETA2**2+H2**2)
      R7=SQRT(ALPHA2**2+BETA2**2+H1**2)
      R8=SQRT(ALPHA2**2+BETA2**2+H2**2)
      F11=(R1+ALPHA1)*(R4+ALPHA2)*(R6+ALPHA1)*(R7+ALPHA2)
      F1=((R2+ALPHA1)*(R3+ALPHA2)*(R5+ALPHA1)*(R8+ALPHA2))/F11
      F22=(R1+BETA1)*(R4+BETA1)*(R6+BETA2)*(R7+BETA2)
      F2=((R2+BETA1)*(R3+BETA1)*(R5+BETA2)*(R8+BETA2))/F22
      F33=(R1+H1)*(R4+H2)*(R6+H2)*(R7+H1)
      F3=((R2+H2)*(R3+H1)*(R5+H1)*(R8+H2))/F33
      F41=ATAN2(ALPHA2*H2,R8*BETA2)
      F42=ATAN2(ALPHA1*H2,R6*BETA2)
      F43=ATAN2(ALPHA2*H2,R4*BETA1)
      F44=ATAN2(ALPHA1*H2,R2*BETA1)
      F45=ATAN2(ALPHA2*H1,R7*BETA2)
      F46=ATAN2(ALPHA1*H1,R5*BETA2)
      F47=ATAN2(ALPHA2*H1,R3*BETA1)
      F48=ATAN2(ALPHA1*H1,R1*BETA1)
      F4=F41-F42-F43+F44-F45+F46+F47-F48
      F51=ATAN2(BETA2*H2,R8*ALPHA2)
      F52=ATAN2(BETA2*H2,R6*ALPHA1)
      F53=ATAN2(BETA1*H2,R4*ALPHA2)
      F54=ATAN2(BETA1*H2,R2*ALPHA1)
      F55=ATAN2(BETA2*H1,R7*ALPHA2)
      F56=ATAN2(BETA2*H1,R5*ALPHA1)
      F57=ATAN2(BETA1*H1,R3*ALPHA2)
      F58=ATAN2(BETA1*H1,R1*ALPHA1)
      F5=F51-F52-F53+F54-F55+F56+F57-F58

  DELTAT(IY,IX)=DELTAT(IY,IX)+(G1*ALOG(F1)+G2*ALOG(F2)+G3*ALOG(F3)
 +
     *G4*F4+G5*F5)*100.0
  100 CONTINUE
  200 CONTINUE
      DO 300 IX=1,LX
```

```
            JX=LX-(IX-1)
   300  WRITE(6,400)(DELTAT(IY,JX),IY=1,LY)
   400  FORMAT(32(F7.0))
            DO 500 IX=1,LX
            X=FLOAT(IX-1)*DELTAX
            DO 500 IY=1,LY
            Y=FLOAT(IY-1)*DELTAY
            WRITE(3,600)Y,X,DELTAT(IY,IX)
   500    CONTINUE
            STOP
    30
FORMAT(F5.1,1X,F6.1,1X,F7.1,1X,2(F7.3,1X),2(F6.3,1X),3(I3,1X))
    40        FORMAT(6(F7.3,1X),F8.5,1X,F5.1,1X,F6.1,1X,F5.1)
   600        FORMAT(1X,F7.2,1X,F7.2,1X,F7.3)
  1000        FORMAT(1X,'INPUT DATA'//1X,'INCL  DECLIN TOTAL F XORIGIN
              YORIGIN
              1 DELTAX DELTAY LX   LY  NBODY')
  1001        FORMAT(1X,F5.1,1X,F6.1,1X,F7.1,1X,2(F7.3,1X),
              2(F6.3,1X),3(I3,1X))
  1002        FORMAT(1X,'BODY       A1        A2
              B1        B2        H1        H2    C
              2GSK      AI0    D0      THETA  J(A/M)')
  1003        FORMAT(1X,I2,3X,6(F7.3,1X),F8.5,1X,F5.1,1X,F6.1,1X,2
              (F5.1,1X))
            END
```

APPENDIX 2
DEPTH ESTIMATES FROM THE LOW FREQUENCY SEDIMENTS TOGETHER WITH
THE COORDINATES OF THE CENTRE OF THE DATA BLOCKS USED FOR
COUNTOURING.

Sheet No.	X-axis (°)	Y-axis (°)	Z-axis (km)	Sheet No.	X-axis (°)	Y-axis (°)	Z-axis (km)
1c	4.125	13.625	.95	29d	5.375	12.625	1.25
1d	4.375	13.625	.45	30a	5.625	12.875	.49
2c	4.625	13.625	.65	30b	5.875	12.875	.69
2d	4.875	13.625	.50	30c	5.625	12.625	.29
3c	5.125	13.625	.71	30d	5.875	12.625	.57
3d	5.375	13.625	.45	31a	6.125	12.875	.40
4c	5.625	13.625	.38	31b	6.375	12.875	.29
4d	5.875	13.625	.65	31c	6.125	12.625	.61
5c	6.125	13.625	.28	31d	6.375	12.625	.85
5d	6.375	13.625	.42	48a	3.625	12.375	.40
8a	4.125	13.375	.53	48b	3.875	12.375	.52
8b	4.375	13.375	.63	48c	3.625	12.125	.44
8c	4.125	13.125	.64	48d	3.875	12.125	.41
8d	4.375	13.125	.53	49a	4.125	12.375	.67
9a	4.625	13.375	.53	49b	4.375	12.375	.35
9b	4.875	13.375	.58	49c	4.125	12.125	.79
9c	4.625	13.125	.64	49d	4.375	12.125	.35
9d	4.875	13.125	.56	50a	4.625	12.375	.69
10a	5.125	13.375	.80	50b	4.875	12.375	.49
10b	5.375	13.375	.55	50c	4.625	12.125	.81
10c	5.125	13.125	.40	50d	4.875	12.125	.71
10d	5.375	13.125	.36	51a	5.125	12.375	.46
11a	5.625	13.375	.74	51b	5.375	12.375	.38
11b	5.875	13.375	.63	51c	5.125	12.125	.66
11c	5.625	13.125	.53	51d	5.375	12.125	.63
11d	5.875	13.125	.57	52a	5.625	12.375	.40
12a	6.125	13.375	.53	52b	5.875	12.375	.28
12b	6.375	13.375	.68	52c	5.625	12.125	.13
12c	6.125	13.125	.31	52d	5.875	12.125	.30
12d	6.375	13.125	1.15	71a	3.625	11.875	.69
26d	3.875	12.625	.36	71b	3.875	11.875	.62
27a	4.125	12.875	.51	71c	3.625	11.625	.40
27b	4.275	12.875	.31	71d	3.875	11.625	.79
27c	4.125	12.625	.50	72a	4.125	11.875	.80
27d	4.375	12.625	.42	72b	4.375	11.875	.71
28a	4.625	12.875	.58	72c	4.125	11.625	.63
28b	4.875	12.875	.68	72d	4.375	11.625	.85
28c	4.625	12.625	.72	73a	4.625	11.875	.29
28d	4.875	12.625	.42	73b	4.875	11.875	.30
29a	5.125	12.875	1.40	73c	4.625	11.625	.90
29b	5.375	12.875	.85	73d	4.875	11.625	.56
29c	5.125	12.625	.85	94a	3.625	11.375	.38

Sheet No.	X-axis (°)	Y-axis (°)	Z-axis (km)	Sheet No.	X-axis (°)	Y-axis (°)	Z-axis (km)
94b	3.875	11.375	.42	96d	4.875	11.125	.59
94c	3.625	11.125	.40	116a	3.625	10.875	.32
94d	3.875	11.125	.31	116b	3.875	10.875	.41
95a	4.125	11.375	.66	116c	3.625	10.625	.40
95b	4.275	11.375	.85	116d	3.875	10.625	.58
95c	4.125	11.125	.96	117a	4.125	10.875	.53
95d	4.375	11.125	.72	117b	4.375	10.875	.85
96a	4.625	11.375	.58	117c	4.125	10.625	.49
96b	4.875	11.375	.28	117d	4.375	10.625	.85
96c	4.625	11.125	.67				